This is to certify that the
thesis entitled

ADAPTIVE RESONANCE TUNING

presented by

Jeffrey Andrew Jeltema

has been accepted towards fulfillment
of the requirements for the

M.S. degree in Mechanical Engineering

C. Goknar
Major Professor's Signature

06/21/05
Date

ADAPTIVE RESONANCE TUNING

By

Jeffrey Andrew Jeltema

A THESIS

Submitted to
Michigan State University
in partial fulfillment of the requirements
for the degree of

MASTER OF SCIENCE

Department of Mechanical Engineering

2005

ABSTRACT

ADAPTIVE RESONANCE TUNING

By

Jeffrey Andrew Jeltema

Resonant systems arise in many areas of science and engineering. Some examples include ultrasonic motors, piezoelectric transducers, induction heating loads, resonant inverter loads, vibrational gyroscopes, cavity resonators and cyclotrons. For optimal performance, these systems must be excited at their resonant frequencies. However, even if resonant and excitation frequencies are initially matched, over time they can drift due to disturbances such as environmental change, load variation, manufacturing variability, fatigue damage, microphonics and electromagnetic detuning, resulting in a loss of performance. This necessitates employment of a resonance tuning control system that maintains lock between the excitation and resonant frequencies.

In this thesis, three resonance tuning methods for lightly damped second order passive loads are investigated. Each method uses the error between the excitation and resonant frequencies obtained by a phase detector to adaptively match these frequencies. In the first method, the excitation to the load is provided by a voltage controlled oscillator, the frequency of which is adaptively tuned. The second method adaptively tunes the resonant frequency of the resonator by changing its structure or element values. Finally, the third method uses proportional feedback around the resonator and adaptively adjusts the feedback gain to tune the closed loop resonant frequency to the excitation frequency. Using the frozen time approach, nonlinear time-varying models that accurately predict the performance of these control systems are developed, and subsequently linearized, to obtain linear time-invariant models that facilitate both analysis and design. Furthermore, stability issues are considered and design guidelines are provided. The results are illustrated through examples.

To my family, Thomas, Linda and Laura

ACKNOWLEDGMENTS

I would like to express my gratitude to my advisor, Dr. Cevat Gökçek, whose expertise and guidance have added considerably to my graduate experience. I truly appreciate the time and effort he has given to me as a research advisor and mentor. I would also like to thank all of my friends and family for their constant support and words of encouragement.

TABLE OF CONTENTS

LIST OF FIGURES

CHAPTER 1

Introduction

Resonant systems arise in many areas of science and engineering. In some cases, these systems must be excited at their resonant frequencies to achieve optimal performance (e.g. resonators) while in some others, excitation of their resonant frequencies may be catastrophic and must be avoided (e.g. bridges). Control systems that achieve the former objective will be referred to as *resonance tuning systems* in this thesis.

1.1 Motivation

Ultrasonic motors, piezoelectric transducers, induction heating loads, some resonant inverter loads, microelectromechanical gyroscopes, cavity resonators and cyclotrons can be modeled as lightly damped second order passive loads [1]–[16]. In order to maximize the average power delivered to such a load or maximize the resonant amplification, it is necessary to drive the load at its resonant frequency [1]–[16]. However, disturbances such as temperature or humidity change, load variation, manufacturing variability, fatigue damage, microphonics and electromagnetic detuning [1]–[16] can cause the resonant frequency or excitation frequency of the load to drift over time and significantly impair the achieved performance. This mandates employment of a resonance tuning system that maintains lock between the excitation frequency and the resonant frequency of the load.

The resonance tuning control problem has received significant attention recently in the contexts of the specific applications listed above and many others. Several

useful analysis and design methods for such systems have been developed and many such systems have been practically implemented [1]–[16]. Despite these encouraging results, development of simple but accurate analysis methods as well as robust and optimal design methods for resonance tuning systems are still needed.

The aim of this thesis is to provide effective tools for modeling, analysis and design of resonance tuning systems. Specifically, resonant systems that can be modelled as lightly damped second order loads will be studied. Since the phase of a second order load takes a constant value ($-\pi/2$, 0 or $+\pi/2$ rad) at its resonant frequency, the main idea in designing the resonance tuning system is to use a phase detector to extract the phase information and use it for feedback purpose. This thesis will investigate three separate resonance tuning methods.

1.2 Problem Formulation

Based on the above motivation, the following three problems are formulated.

Modeling Problem: Given a resonator, develop an overall model that includes the resonator and an appropriate resonance tuning system.

Analysis Problem: Given an overall model of a resonator and a resonance tuning system, determine the performance of the feedback system (stability, robustness, disturbance rejection, reference tracking, rise time, settling time, maximum overshoot, etc.); also determine performance limitations and tradeoffs.

Design Problem: Given an overall model of a resonance tuning system, design the parameters so that the system achieves certain desired performance objectives.

Although the resonators mentioned above can be similarly modeled, they differ from each other as to what part of the system actuation is possible. In this thesis, resonance tuning systems will be classified into three groups based on actuation

possibilities.

Group 1: This group consists of those systems that allow actuation on the excitation frequency. That is, these systems contain means to adaptively tune the excitation frequency to the resonant frequency of the resonator. It should be noted that with this case, actuation on the resonant frequency may or may not be possible.

Group 2: This group of systems consists of those that allow actuation on the resonant frequency. This requires the ability to adjust a parameter or element value of the resonator on which the resonant frequency is dependant. It should be noted that with this case, actuation on the excitation frequency may or may not be possible.

Group 3: Finally, the last group consists of systems where actuation on neither the excitation frequency, nor the resonant frequency is practical.

For each group of resonators, this thesis will present an appropriate resonance tuning system and provide solutions to the three problems formulated above. The resonance tuning systems will be demonstrated with simulations.

1.3 Resonance Tuning Systems

This section introduces the three resonance tuning systems considered in this thesis. Some representative examples are also provided.

1.3.1 RTS1

The first resonance tuning system assumes the resonator fits into actuation group 1 above. That is, actuation on the excitation frequency is possible. In this resonance tuning system, the source of excitation is a voltage controlled oscillator (VCO). A phase detector is used to produce an error signal that is proportional to the error between excitation and resonant frequencies. This error signal is then used to adap-

tively tune the output frequency of the VCO in a direction to reduce the error between excitation and resonant frequencies. The combination of a phase detector and a VCO is known as a phase locked loop (PLL). The PLL is a common tool in many communication systems, however, use of the PLL for the purpose of resonance tuning is a fairly recent idea.

Some physical systems where RTS1 may be implemented include some fluorescent lighting loads, induction heating loads, piezoelectric transducers or ultrasonic motors. The exact frequency at which these systems resonate is not important, only that they achieve resonance within a reasonable range. Thus RTS1 is well suited for these applications.

One physical system that currently implements RTS1 is a plasma ignition system. Although this ignition system is still being developed, early results have shown that when RTS1 is implemented, the system can maintain resonance despite changes in its resonant frequency.

The basic principle of this plasma ignition system is to use resonance boosting to achieve the required high voltage for the breakdown and sustain the plasma by continuing RF excitation. This ignition system generates a strong RF plasma torch for a prescribed duration and hence it is expected to achieve faster, more uniform and more complete combustion. Prior to discharge, a spark plug is basically a very small cylindrical capacitor. Connecting an inductor in series with the spark plug forms a series resonant circuit. A model of the plasma ignition system is shown in Figure 1.1. In this figure, the lightly damped second order load is the series RLC circuit and the rest of the circuit provides the excitation. Driving this circuit with a suitable RF generator exactly at its resonant frequency yields a very high RF voltage across the spark plug and results in an RF plasma torch. However, due to environmental changes, the resonant frequency may drift with time, thus impairing the the performance of the system significantly. Hence a resonance tuning system is

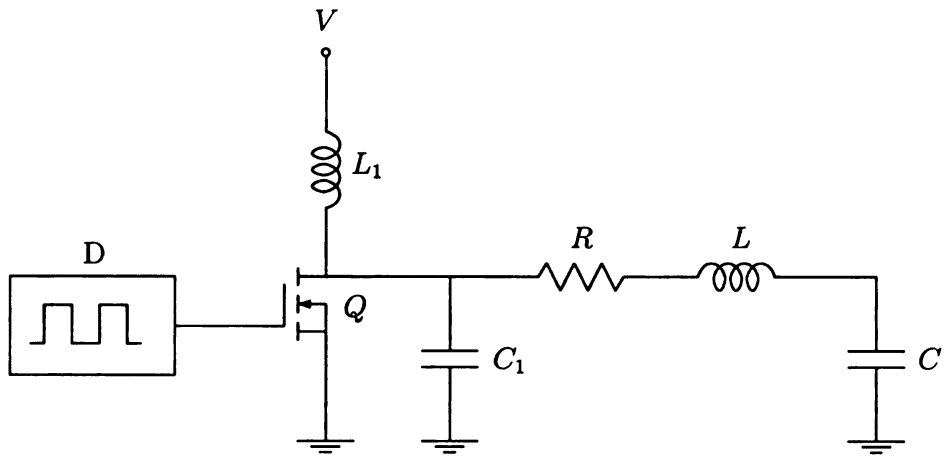

Figure 1.1. Plasma ignition system.

required. As the plasma ignition system fits into actuation group 1 above, RTS1 is implemented.

1.3.2 RTS2

The second resonance tuning system considered assumes the resonator fits into actuation group 2. That is, actuation is possible on a parameter of the resonator that changes the resonant frequency. Again, a phase detector is used to determine the error between excitation and resonant frequencies. This error is then used to adaptively tune a parameter of the resonator so that the resonant frequency varies in a direction that reduces the error between the resonant and excitation frequencies.

RTS2 is well suited for use in wireless communication devices. In these devices, for instance cellular phones, the frequency of an incoming signal cannot be adjusted. Hence, to achieve optimal performance, the center frequency of the bandpass filter within the phone must be adjusted. This can be accomplished by implementing RTS2.

Another physical system well suited for RTS2 is a cavity resonator. The resonant

frequencies of these resonators are required to be precisely tuned to their excitation frequencies as they typically have high quality factors. However, their resonant frequencies can easily drift during operation due to factors such as temperature change, humidity change or microphonics. The result is a large decrease in the performance of these resonators. Thus, a resonance tuning system is required. RTS2 is well suited to cavity resonators due to the fact that the resonant frequency of a cavity resonator depends on the cavity dimensions. Thus, the resonant frequency of these systems can be tuned by altering their physical dimensions. These adjustments can be accomplished, for instance, with piezoelectric actuators [8]–[12].

1.3.3 RTS3

The third resonance tuning system considered assumes the resonator fits into actuation group 3 above. That is, actuation is possible on neither the excitation frequency nor the resonant frequency. Instead, a feedback loop is introduced around the resonator to allow for the tuning of the closed loop resonant frequency. Similar to RTS1 and RTS2, a phase detector is used to determine the error between excitation and closed loop resonant frequencies. This error is then used to adaptively tune the feedback gain, and thus tune the closed loop resonant frequency, in a direction that reduces the error between excitation and closed loop resonant frequencies.

An example of a physical system where this method is well suited is a vibrational gyroscope. Vibrational gyroscopes measure the angular velocity of a rotating system by sensing the Coriolis force on the system. They are basically a mass spring damper system driven to vibrate in one direction. When the gyroscope rotates, the Coriolis force causes the mass to move in a direction perpendicular to the drive axis and rotation axis [6]. In order to obtain a large response, most gyroscopes must be driven at their resonant frequency. However, due to manufacturing variability, temperature and aging the resonance condition can easily be lost. Thus, a resonance tuning

system is required. Typical MEMS gyroscopes utilize a PLL to tune the excitation frequency to the resonant frequency of the gyroscope [6]. However, this method does not allow for the operating frequency to be chosen by the designer, which means this frequency cannot be used in the signal processing design. Instead RTS3, which creates a feedback loop around the resonator and adaptively tunes the feedback gain to bring the closed loop resonant frequency to match the excitation frequency can be utilized.

1.4 Thesis Overview

1.4.1 Organization

This thesis is organized as follows: Chapter 2 provides the models of the three resonance tuning systems considered in this work as well as the models of a generic resonator and two types of phase detectors. Chapter 3 provides analysis of the three resonance tuning systems including model simplification and stability results. Chapter 4 discusses the issues surrounding the design of these resonance tuning systems and provides simulation results of each resonance tuning system. Chapter 5 presents a byproduct of this study, adaptively enhanced phase locked loops. Finally, in Chapter 6, conclusions are given as well as some future research directions.

1.4.2 Original Contributions

The main contribution of this thesis is the development of systematic analysis and design methods for the adaptive resonance tuning systems described above. Specifically, assuming that the parameters of a lightly damped second order passive load (including its resonant frequency) and its excitation frequency vary slowly with time, nonlinear time-varying models that accurately predict the performance of these res-

onance tuning systems are developed. These developed models are subsequently linearized to obtain linear time-invariant models that predict the performance of these systems. Furthermore, stability analysis of the nonlinear and linear models is carried out. Finally, based on the developed linear time-invariant models, guidelines for designing the resonance tuning systems are provided.

The research in this thesis has generated three published works [19]–[21]. Also, another paper providing a summary of the research on adaptive resonance tuning systems presented in this thesis is currently in preparation.

CHAPTER 2

Modeling

2.1 Introduction

In this chapter, models are presented for the three resonance tuning systems introduced in Chapter 1. Also presented is a review of the phase detectors used in this thesis and the model of a generic resonator.

As stated earlier, the resonance tuning systems considered in this thesis apply to resonators that are lightly damped second order passive loads. Since any lightly damped second order load can be modeled as a series RLC circuit, this thesis will repeatedly use series RLC circuits for the purpose of illustration. It should be noted that in most of the examples provided in this work, the nominal element values of this circuit will not accurately represent any physical system. However, this fact does not devalue the examples since time can be scaled without changing the qualitative response of the resonance tuning systems. The response of these system is, however, dependant on the quality factor of the resonator. Therefore, examples covering a variety of quality factors will be considered throughout this work.

The remainder of this chapter is organized as follows. In Section 2.2, the model of a resonator is considered. In Section 2.3, two types of phase detectors are discussed. Finally, in Section 2.4, the three methods of resonance tuning are investigated.

2.2 Resonator Model

The dynamics of a lightly damped second order system are governed by the differential equation

$$\ddot{y}(t) + 2\zeta(t)\omega_n(t)\dot{y}(t) + \omega_n^2(t)y(t) = k_g\omega_n^2(t)u(t), \tag{2.1}$$

where $u(t)$ is the input, $y(t)$ is the output, $\omega_n(t)$ is the resonant frequency, $\zeta(t)$ is the damping ratio and k_g is the input gain. The input to the system $u(t)$ is assumed to be in the form

$$u(t) = A\cos\left[\omega_0 t + \theta(t)\right], \tag{2.2}$$

where A is the amplitude, ω_0 is the nominal angular frequency and $\theta(t)$ is the instantaneous phase of the input. It then follows that the instantaneous frequency of the input is

$$\omega_s(t) = \omega_0 + \dot{\theta}(t). \tag{2.3}$$

Thus, optimal performance requires $\omega_s(t)$ to be equal to the resonant frequency of the resonator.

2.2.1 Resonant Frequency

The way in which the resonant frequency of a lightly damped second order system is defined varies throughout the different disciplines of science and engineering. Certain applications consider a system in resonance when maximum power transfer is achieved, while in others, maximum signal amplification defines resonance. In this thesis, we will define the resonant frequency ω_r as the frequency at which maximum power transfer occurs. For lightly damped second order systems, it follows that

$$\omega_r = \omega_n. \tag{2.4}$$

We will define the frequency at which maximum signal amplification occurs as the peak frequency ω_p. For lightly damped second order systems, the value of ω_p depends on where the system output is taken.

To help illustrate this, consider a series RLC circuit as the resonator. This circuit is as shown in Figure 2.1, where R, L and C are a resistor, inductor and capacitor, respectively, and $u(t)$ and $y(t)$ are the input and output, respectively. In Figure 2.1,

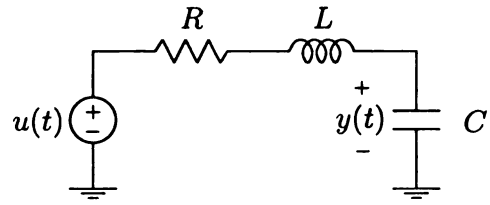

Figure 2.1. Model of the RLC circuit.

the output $y(t)$ is taken as the voltage across the capacitor. The resulting transfer function $H_C(s)$ is

$$H_C(s) = \frac{\omega_n^2}{s^2 + 2\zeta\omega_n s + \omega_n^2}, \tag{2.5}$$

where

$$\omega_n = \frac{1}{\sqrt{LC}} \tag{2.6}$$

and

$$\zeta = \frac{R}{2}\sqrt{\frac{C}{L}}. \tag{2.7}$$

From the definition above, it follows that the peak frequency is the frequency at which $|H_C(j\omega)|$ is a maximum. By taking the derivative of $|H_C(j\omega)|$ with respect to $j\omega$ and

setting it equal to zero, it follows that the the peak frequency ω_p is

$$\omega_p = \omega_n\sqrt{1-2\zeta^2}. \tag{2.8}$$

However, the output can also be taken as the voltage across the resistor or inductor. Taking $y(t)$ as the voltage across the resistor results in the transfer function

$$H_R(s) = \frac{2\zeta\omega_n s}{s^2+2\zeta\omega_n s+\omega_n^2}. \tag{2.9}$$

Again defining the peak frequency as before, it follows that

$$\omega_p = \omega_n. \tag{2.10}$$

Furthermore, taking y as the voltage across the inductor results in the transfer function

$$H_L(s) = \frac{s^2}{s^2+2\zeta\omega_n s+\omega_n^2}. \tag{2.11}$$

In this case, the peak frequency is

$$\omega_p = \frac{\omega_n}{\sqrt{1-2\zeta^2}}. \tag{2.12}$$

To illustrate these transfer functions, consider the RLC circuit with values of R, L and C as R=5 Ω, L=10 mH and C=100 μF. Thus, ω_n=1000 rad/s and $\zeta = 0.25$. The bode plots of $H_C(j\omega)$, $H_R(j\omega)$ and $H_L(j\omega)$ are shown in Figure 2.2, Figure 2.3 and Figure 2.4, respectively. As seen in these plots, it is evident that the phase at which ω_p or ω_r occur, is dependant on where the system output is taken. This value determines what type of phase detector may be used in the resonance tuning system. More discussion of phase detectors is provided in Section 2.3.

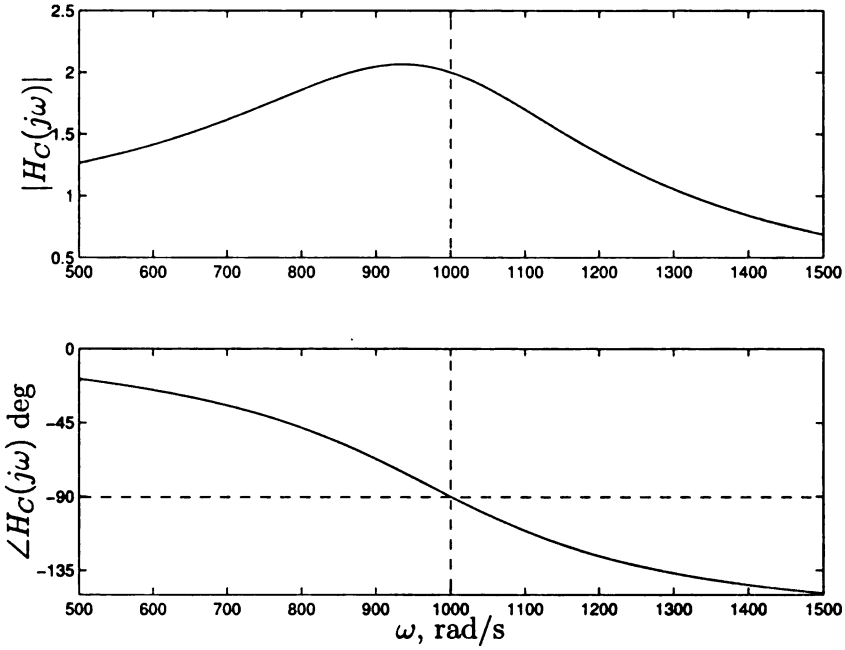

Figure 2.2. Bode plot of the $H_C(j\omega)$.

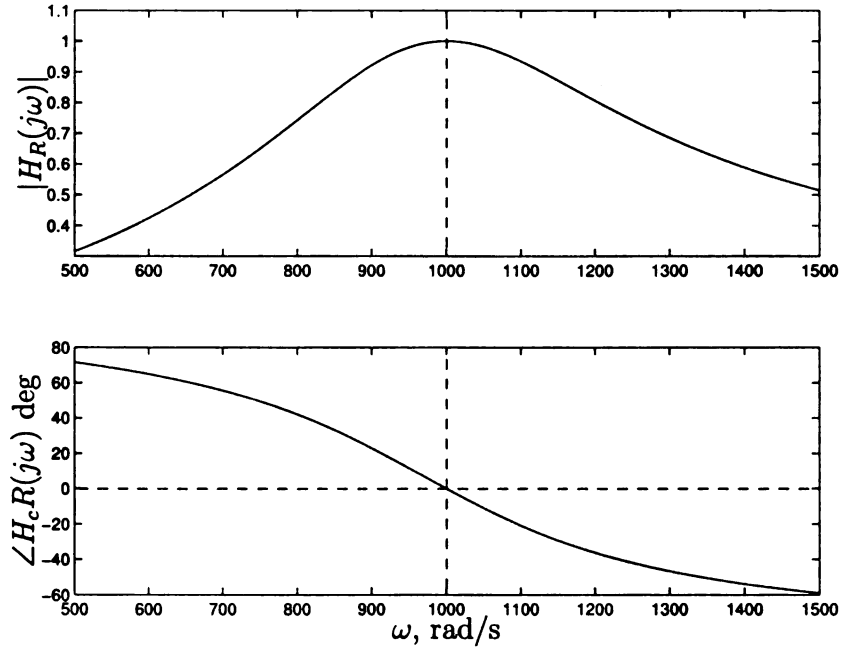

Figure 2.3. Bode plot of the $H_R(j\omega)$.

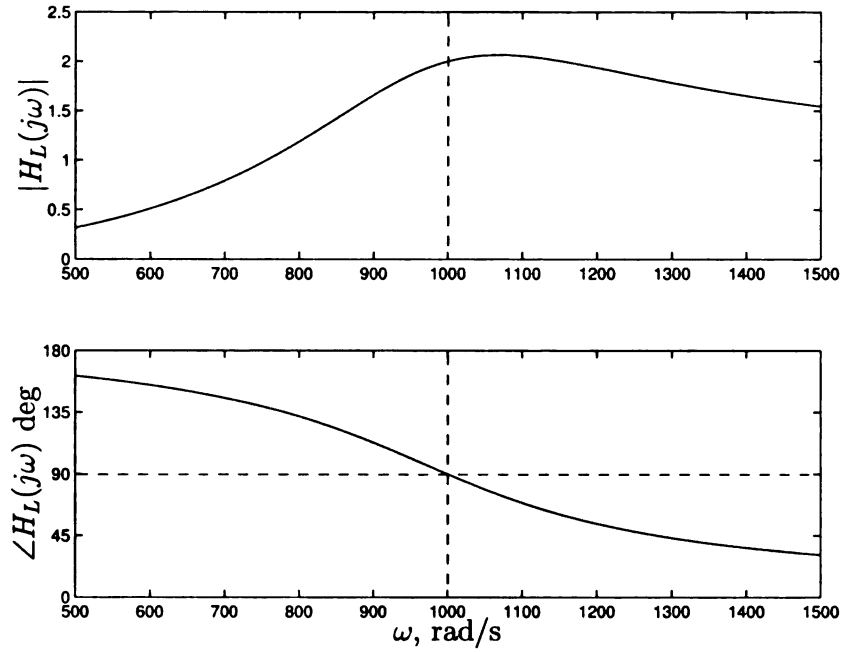

Figure 2.4. Bode plot of the $H_L(j\omega)$.

Despite the different definitions provided above, for all resonance tuning applications, this thesis assumes optimal performance always occurs when (2.4) is satisfied. This is possible due the nature of the systems we will be considering. In these systems, the damping ratio is very small and therefore ω_r, ω_p and ω_n are all practically equal. For the remainder of this work, we will refer to any of these three frequencies simply as the *resonant frequency.*

2.2.2 Effects of Detuning

Depending on the quality factor of a resonator operating at resonance, a very slight change in either the resonant or excitation frequency can cause a very large decrease in the system output.

To illustrate this fact, consider a series RLC circuit and assume the nominal values of R, L and C are $R_0 = 0.25\ \Omega$, $L_0 = 0.1$ H and $C_0 = 10\ \mu$F, respectively, so that

the nominal values of ω_n, ζ and Q are $\omega_0 = 1000$ rad/s, $\zeta_0 = 0.00125$ and $Q_0 = 400$, respectively. A Bode plot of this resonator is shown in Figure 2.5. Due to the

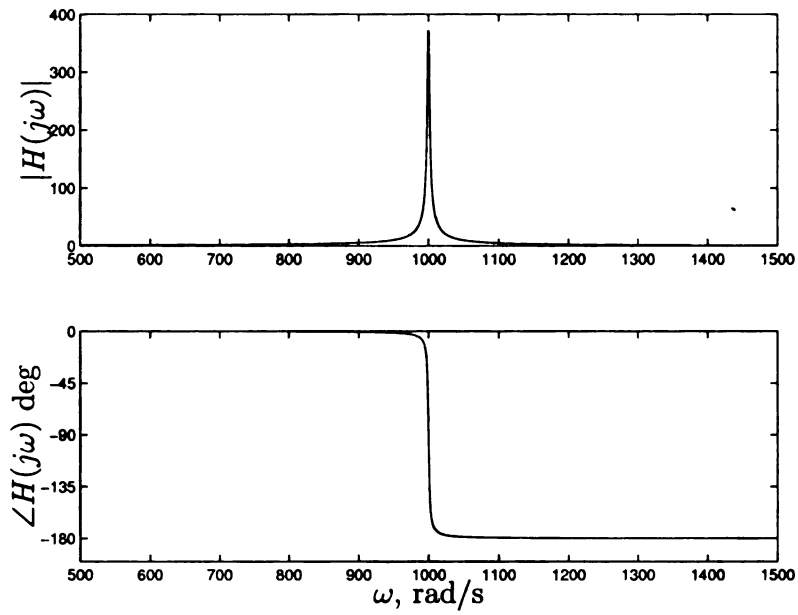

Figure 2.5. Bode plot of RLC example.

sharpness of the peak in this figure, even slight detuning from the resonant frequency is expected to cause a significant decrease in the resonator output. This can be seen in Figures 2.6 and 2.7 which are plots of output voltage across the capacitor versus time. In Figure 2.6 the resonator is excited at its resonant frequency which results in a steady state output of 400 V across the capacitor. However, in Figure 2.7, the value of C is decreased by 1 percent, so that the resonant frequency $\omega_n(t)$ becomes 1005.04 rad/s, while the excitation frequency remains 1000 rad/s. These figures show that a change of only 0.5 percent in the resonant frequency causes the steady state output voltage to decrease by 75 percent from 400 V to 100 V.

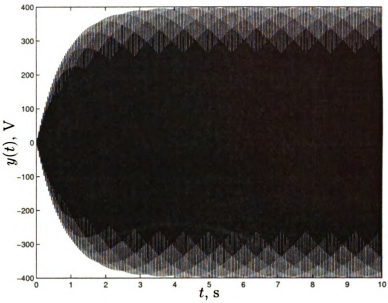

Figure 2.6. Output of uncontrolled resonator excited at $\omega_n(t)$.

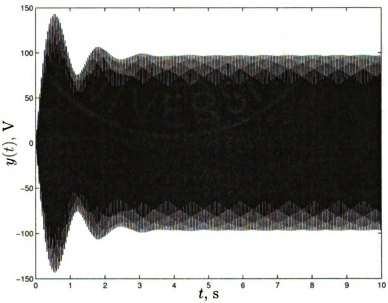

Figure 2.7. Output of uncontrolled resonator with 1 percent drop in capacitance.

With such a decrease in output, the resonator is obviously far from optimal performance. Therefore, a method is clearly needed to control the resonant or excitation frequency.

2.3 Phase Detectors

The previous discussion necessitates employment of a resonance tuning system that maintains $\omega_s(t)$ and $\omega_n(t)$ as close to each other as possible despite changes in either frequency. In order to achieve this task, the controller must have means to sense the error between these frequencies. As mentioned earlier, a phase detector can be used to sense the error.

A phase detector compares the phases of two signals applied to its inputs and generates an output signal whose average value is related to the phase difference between these input signals [24, 25]. This output is also a measure of frequency difference, as signals with differing frequencies cannot be locked in phase unless one is a harmonic of the other.

There exist several types of phase detectors with different characteristics. The phase detectors considered in this thesis are a multiplication type analog phase detector and an exor type digital phase detector. Below, these two types of phase detectors will be reviewed briefly.

2.3.1 Multiplication Phase Detector

A multiplication type phase detector uses an analog multiplier phase comparator followed by a lowpass filter to extract the phase information at its inputs as shown in Figure 2.8. In this figure, the signals $v_1(t)$ and $v_2(t)$ are the inputs, $v(t)$ is the output, $F(s)$ is the transfer function of the lowpass filter and $\times$ is the multiplication operation.

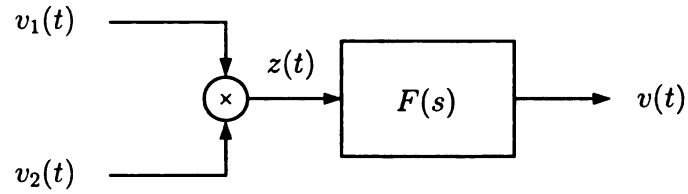

Figure 2.8. Model of the multiplication phase detector.

Assuming that $v_1(t)$ and $v_2(t)$ are in the forms

$$v_1(t) = A_1(t)\cos\left[\omega_0 t + \theta_1(t)\right] \tag{2.13}$$

and

$$v_2(t) = A_2(t)\cos\left[\omega_0 t + \theta_2(t)\right], \tag{2.14}$$

where $A_1(t) > 0$ and $A_2(t) > 0$ are the instantaneous amplitudes, $\theta_1(t)$ and $\theta_2(t)$ are the instantaneous phases and ω_0 is the nominal angular frequency, it follows that

$$z(t) = \frac{A_1(t)A_2(t)}{2}\cos\left[\theta_2(t) - \theta_1(t)\right] + \frac{A_1(t)A_2(t)}{2}\cos\left[2\omega_0 t + \theta_2(t) + \theta_1(t)\right]. \tag{2.15}$$

Assuming further that $A_1(t)$, $A_2(t)$, $\theta_1(t)$ and $\theta_2(t)$ vary slowly with time compared to the time variation of $\omega_0 t$ (i.e., $|\dot{A}_1(t)| \ll \omega_0$, $|\dot{A}_2(t)| \ll \omega_0$, $|\dot{\theta}_1(t)| \ll \omega_0$ and $|\dot{\theta}_2(t)| \ll \omega_0$) and that the lowpass filter completely removes the high frequency term around $2\omega_0$, the phase detector output $v(t)$ can be written as

$$v(t) = f(t) * \varphi_m\left[\theta_2(t) - \theta_1(t)\right], \tag{2.16}$$

where

$$\varphi_m\left[\theta(t)\right] = \frac{A_1(t)A_2(t)}{2}\cos\left[\theta(t)\right], \tag{2.17}$$

$f(t)$ is the impulse response of the lowpass filter and $*$ is the convolution operation. Figure 2.9 shows $\varphi_m[\theta(t)]$ as a function of $\theta(t) = \theta_2(t) - \theta_1(t)$, where the amplitude $[A_1(t)A_2(t)]/2$ is normalized to A.

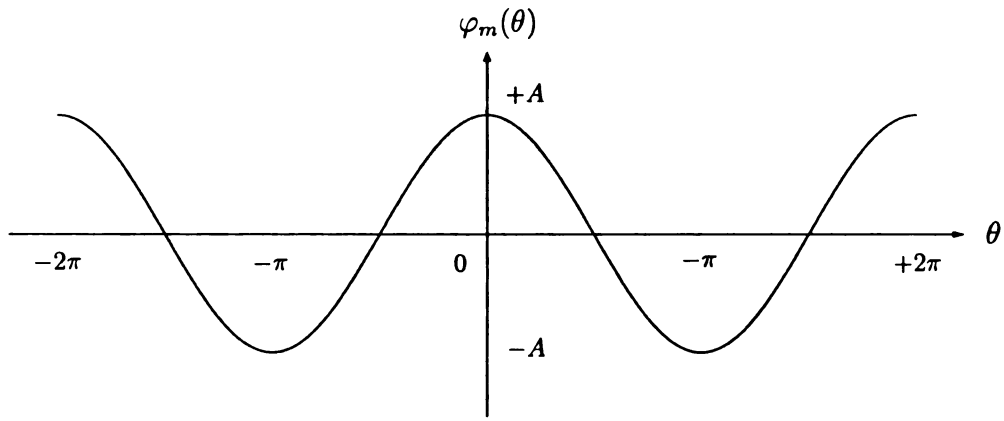

Figure 2.9. Multiplication phase comparator characteristic.

The nonlinear equation (2.17) describes the operation of the multiplication type phase detector very accurately provided that the assumptions made earlier are satisfied. Note that the amplitudes of both input signals affect the output of the phase detector. This must be accounted for when designing the gains in the system. As will be shown next, the amplitudes of the input signals do not affect the output of the exor type phase detector.

2.3.2 Exor Phase Detector

An exor type phase detector uses a digital exor phase comparator followed by a lowpass filter to extract the phase information at its inputs as shown in Figure 2.10. In this figure, the signals $v_1(t)$ and $v_2(t)$ are the inputs, $v(t)$ is the output, $F(s)$ is the transfer function of the lowpass filter, $\oplus$ is the exor logic gate with logic 0 and 1

levels being $-V$ and $+V$, respectively, and HLs are hard limiters with limiting levels $\pm V$ that convert the signals $v_1(t)$ and $v_2(t)$ at the input of phase detector into the digital signals $u_1(t)$ and $u_2(t)$.

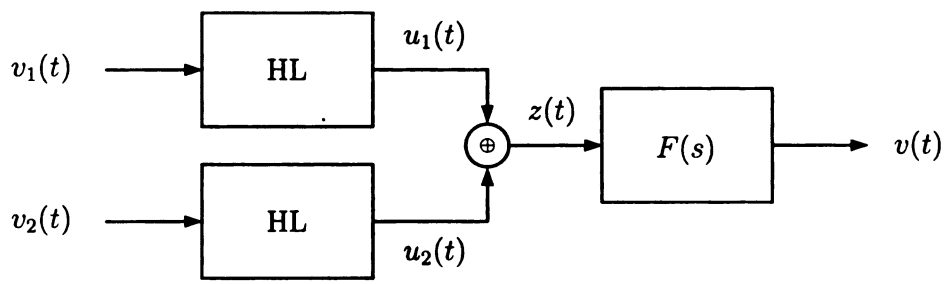

Figure 2.10. Model of the exor phase detector.

Assuming that the inputs $v_1(t)$ and $v_2(t)$ are as before, the signals $u_1(t)$ and $u_2(t)$ can be expressed as

$$u_1(t) = V \operatorname{sgn}\left(\cos\left[\omega_0 t + \theta_1(t)\right]\right) \tag{2.18}$$

and

$$u_2(t) = V \operatorname{sgn}\left(\cos\left[\omega_0 t + \theta_2(t)\right]\right). \tag{2.19}$$

Thus, it follows that

$$z(t) = u_1(t) \oplus u_2(t). \tag{2.20}$$

Similar to the previous case, assuming that both $\theta_1(t)$ and $\theta_2(t)$ vary slowly with time compared to the time variation of $\omega_0 t$ (i.e., $|\dot{\theta}_1(t)| \ll \omega_0$ and $|\dot{\theta}_2(t)| \ll \omega_0$), the signal $z(t)$ can be expressed as

$$z(t) = \varphi_e\left[\theta_2(t) - \theta_1(t)\right] + r(t), \tag{2.21}$$

where $\varphi_e\left[\theta(t)\right]$ as a function of $\theta(t) = \theta_2(t) - \theta_1(t)$ is as shown in Figure 2.11 and the

term $r(t)$ includes the high frequency components that occur around $2\omega_0$, $4\omega_0$, and so on. Assuming further that the lowpass filter $F(s)$ completely removes the high

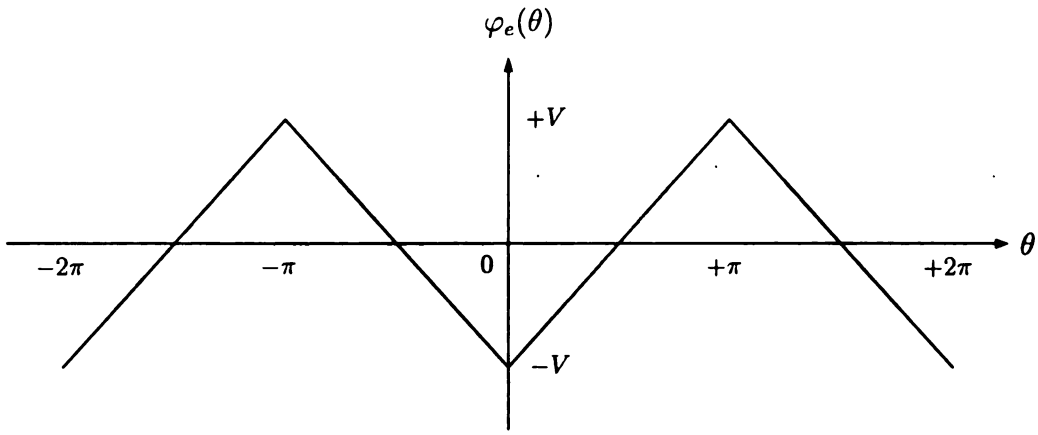

Figure 2.11. Exor phase comparator characteristic.

frequency term $r(t)$, the output of the phase detector $v(t)$ is given by

$$v(t) = f(t) * \varphi_e\left[\theta_2(t) - \theta_1(t)\right], \tag{2.22}$$

where $f(t)$ is the impulse response of the lowpass filter and $*$ is the convolution operation.

Like the previous case, this nonlinear equation governs the operation of the phase detector very accurately provided that the assumptions stated above are satisfied. Moreover, note that the output of phase detector $v(t)$ is also a slowly time-varying signal.

2.4 Resonance Tuning Systems

The following subsections provide models of the three resonance tuning systems introduced in Chapter 1.

2.4.1 RTS1

As discussed earlier, RTS1 is a PLL based resonance tuning system. A block diagram of RTS1 is shown in Figure 2.12. In this figure, SYS is a resonator, PD is a phase detector, VCO is a voltage controlled oscillator, $u(t)$ is the VCO output, $y(t)$ is the resonator output and $v(t)$ is the phase detector output.

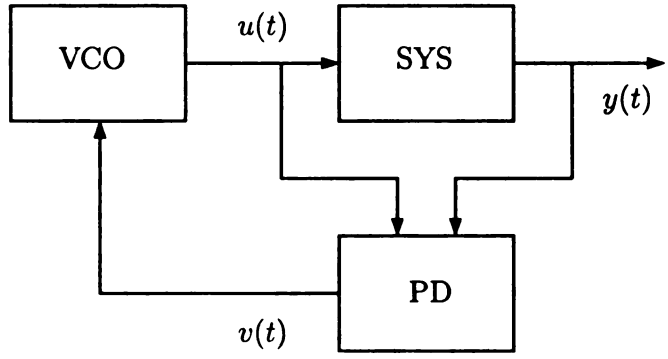

Figure 2.12. Model of RTS1.

A model of the VCO is shown in Figure 2.13, where ω_0 is the center frequency and k_ω is the angular frequency gain. Defining

$$\dot{\theta}_1(t) = k_\omega v(t), \tag{2.23}$$

the signal $u(t)$ may be written as

$$u(t) = V \cos\left[\omega_0 t + \theta_1(t)\right], \tag{2.24}$$

where V is the amplitude. If a digital VCO is used, this signal becomes the Walsh function

$$u(t) = V \operatorname{sgn}\left(\cos\left[\omega_0 t + \theta_1(t)\right]\right). \tag{2.25}$$

It should be noted that the narrow bandpass nature of a resonator will essentially reject all but the first harmonic of the input signal. Thus, if a sinusoidal function or Walsh function are input to a resonance tuning system, the response of the resonator will remain generically the same.

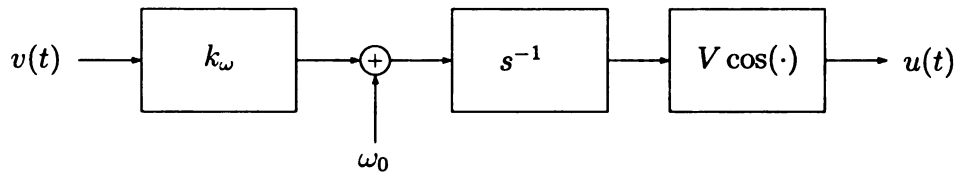

Figure 2.13. Model of the voltage controlled oscillator.

Assuming the resonator model described above, the output $y(t)$ satisfies the differential equation

$$\ddot{y}(t) + 2\zeta(t)\omega_n(t)\dot{y}(t) + \omega_n^2(t)y(t) = \omega_n^2(t)u(t), \tag{2.26}$$

where $\omega_n(t)$ is the natural frequency of the resonator and $\zeta(t)$ is the damping ratio. Assuming the instantaneous frequency of the input is $\omega_s(t)$, the goal of RTS1 is to keep $\omega_s(t)$ as close to $\omega_n(t)$ as possible despite disturbances due to environmental

changes, by adaptively tuning $\omega_s(t)$.

2.4.2 RTS2

As mentioned in Chapter1, RTS2 adaptively controls the resonant frequency of a resonator by changing the structure of the resonator. To help illustrate RTS2, a series RLC circuit is again considered as the resonator. A block diagram of RTS2 is shown in Figure 2.14, where $R(t)$, $L(t)$ and $D(t)$ form the tunable resonator and PD is a phase detector.

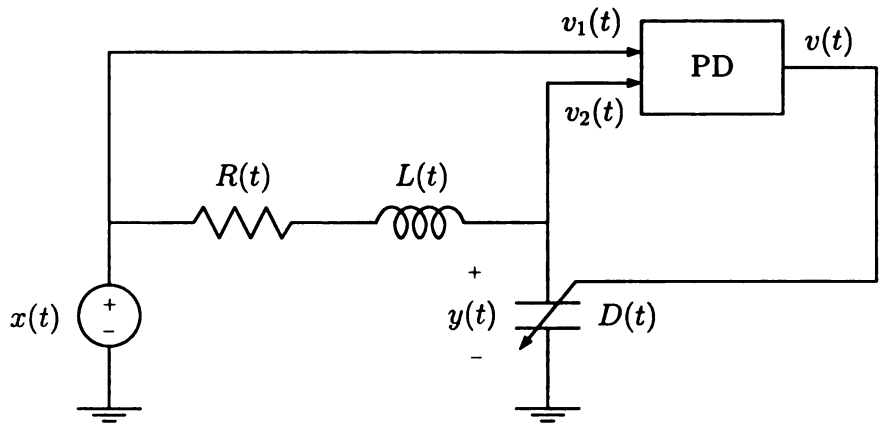

Figure 2.14. Model of the RTS2.

The resonance tuning is achieved by adaptively controlling the resonant frequency through the variable capacitor $D(t)$ using the error between the excitation frequency and resonant frequency. As stated before, the resonant frequency of a series RLC circuit is

$$\omega_n(t) = \frac{1}{\sqrt{L(t)C(t)}}. \tag{2.27}$$

However, in the resonator being considered, it is assumed that the capacitance $D(t)$

is controlled by the output of the phase detector $v(t)$ about its uncontrolled value $C(t)$ according to the expression

$$D(t) = \frac{C(t)}{1 + k_\omega v(t)}, \tag{2.28}$$

where k_ω is an appropriate constant. With this tunable capacitor, the new resonant frequency of the resonator becomes

$$\omega_c(t) = \omega_n(t)\sqrt{1 + k_\omega v(t)}. \tag{2.29}$$

Similarly, the new damping ratio of the resonator becomes

$$\xi(t) = \frac{\zeta(t)}{\sqrt{1 + k_\omega v(t)}}. \tag{2.30}$$

Thus, assuming $R(t)$, $L(t)$ and $D(t)$ vary slowly with time, the voltage $y(t)$ across the capacitor satisfies the differential equation

$$\ddot{y}(t) + 2\zeta(t)\omega_n(t)\dot{y}(t) + \omega_c^2(t)y(t) = \omega_c^2(t)x(t). \tag{2.31}$$

Hence, the goal of the resonance tuning system is to keep $\omega_c(t)$ as close to $\omega_s(t)$ as possible through $v(t)$, despite disturbances due to environmental changes.

2.4.3 RTS3

As previously stated, RTS3 does not directly actuate on resonant or excitation frequency. Instead, this system places the resonator in a feedback loop, and the feedback gain is adaptively adjusted to bring the resonant frequency of the closed-loop system to match the excitation frequency. A model of RTS3 is shown in Figure 2.15.

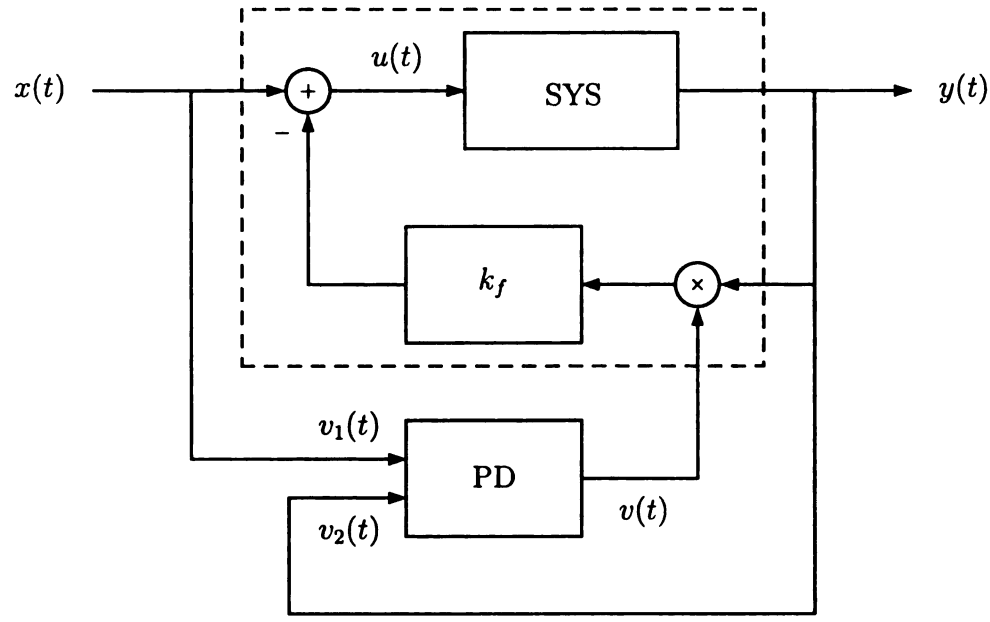

Figure 2.15. Model of RTS3.

In this figure, SYS is the lightly damped second order system, PD is the phase detector, k_f is the feedback gain and $x(t)$ is the external input to the system. It follows from this figure that

$$u(t) = x(t) - k_f v(t) y(t), \tag{2.32}$$

where $v(t)$ is the error signal generated by the phase detector. Thus, the differential equation governing the closed-loop system inside the dashed box can be written as

$$\ddot{y}(t) + 2\zeta(t)\omega_n(t)\dot{y}(t) + \left[1 + k_f k_g v(t)\right]\omega_n^2(t) y(t) = k_g \omega_n^2(t) x(t). \tag{2.33}$$

The resonant frequency of this system is

$$\omega_c(t) = \omega_n(t)\sqrt{1 + k_\omega v(t)}, \tag{2.34}$$

where $k_\omega = k_f k_g$. Hence, the goal of the resonance tuning system is to keep $\omega_c(t)$ as close to $\omega_s(t)$ as possible through $v(t)$, despite changes in the excitation frequency or resonant frequency of the resonator.

CHAPTER 3

Analysis

3.1 Introduction

In this section, the models developed in Chapter 2 are considered and analysis methods are developed. For this purpose, the slow time-varying approach [26, 27, 28] is adopted. Since it is assumed that the resonator parameters are slowly time-varying compared to its excitation, this approach is justified.

For each resonance tuning system, a nonlinear time-varying model that accurately predicts the performance of the resonance tuning system is developed. This developed model is subsequently linearized to obtain a linear time-invariant model that facilitates both analysis and design of the resonance tuning system. Stability results of the developed models are also provided.

The remainder of this chapter is organized as follows. In Section 3.2, the developed models are simplified. In Section 3.3, stability issues are considered.

3.2 Analysis

In this section, models of the three resonance tuning systems are analyzed and simplified. For each resonance tuning system, either a digital exor phase detector or an analog multiplication phase detector is used. However, the methods presented in this work can be easily extended if a phase detector other than the one illustrated here is used.

3.2.1 RTS1

Consider the resonance tuning system shown in Figure 2.12 and assume that PD is an exor type phase detector. Assume further that the VCO output $u(t)$ is in the form of (2.25), where ω_0 is the angular frequency and $\theta_1(t)$ is the instantaneous phase. The instantaneous frequency of the input is then

$$\omega_s(t) = \omega_0 + \dot{\theta}_1(t). \tag{3.1}$$

Under these assumptions, the output $y(t)$ satisfies the differential equation (2.26). Since this equation is time varying, it is impossible to find the voltage $y(t)$ analytically. However, with the frozen time assumption, the parameters $\omega_n(t)$, $\zeta(t)$, and $\theta_1(t)$ can be treated as constant but unknown, and the transfer function from $u(t)$ to $y(t)$ can be expressed as

$$H(s) = \frac{\omega_n^2(t)}{s^2 + 2\zeta(t)\omega_n(t)s + \omega_n^2(t)}. \tag{3.2}$$

The output $y(t)$ can then be approximated at steady state as

$$y(t) = A_2(t)\cos\left[\omega_0 t + \theta_2(t)\right] + e(t), \tag{3.3}$$

where $A_2(t) = 4V|H[j\omega_s(t)]|/\pi$, $\theta_2(t) = \theta_1(t) + \angle H[j\omega_s(t)]$ and $e(t)$ includes the higher order harmonics that occur at $3\omega_s(t)$, $5\omega_s(t)$ and so on. Assuming the quality factor of the resonator is sufficiently high (greater than 10), these higher order harmonics can be neglected, and $y(t)$ can be approximated as

$$y(t) = A_2(t)\cos\left[\omega_0 t + \theta_2(t)\right]. \tag{3.4}$$

Thus, with $u(t)$ and $y(t)$ the inputs to the exor phase detector, it follows from (2.22) that the output $v(t)$ is

$$v(t) = f(t) * \varphi_e \angle H[j\omega_s(t)], \tag{3.5}$$

where $f(t)$ is the impulse response of the lowpass filter and $*$ is the convolution operation. Since $-\pi < \angle H[j\omega_s(t)] \leq 0$, it follows from the phase comparator characteristic that

$$v(t) = f(t) * k_\theta \left(-\angle H[j\omega_s(t)] - \pi/2\right), \tag{3.6}$$

where $k_\theta = 2V/\pi$ is the gain of the phase detector. Combining (2.23) with (3.6), and using

$$\angle H[j\omega_s(t)] = -\arctan\left[\frac{2\zeta(t)\omega_n(t)\omega_s(t)}{\omega_n^2(t) - \omega_s^2(t)}\right], \tag{3.7}$$

it follows that

$$\dot{\theta}_1(t) = k_\omega f(t) * k_\theta \arctan\left[\frac{\omega_n^2(t) - \omega_s^2(t)}{2\zeta(t)\omega_n(t)\omega_s(t)}\right]. \tag{3.8}$$

Combining this equation with (3.1) results in

$$\omega_s(t) - \omega_0 = k_\omega f(t) * k_\theta \arctan\left[\frac{\omega_n^2(t) - \omega_s^2(t)}{2\zeta(t)\omega_n(t)\omega_s(t)}\right]. \tag{3.9}$$

Although simulation shows that (3.9) characterizes the RTS1 very accurately, it is nonlinear and time-varying, and thus, it has limited value. Hence, this equation is linearized below to obtain a more tractable linear time-invariant model.

Let $\delta\omega_n(t) = \omega_n(t) - \omega_0$ and $\delta\omega_s(t) = \omega_s(t) - \omega_0$ be the deviations of $\omega_n(t)$ and $\omega_s(t)$ from the nominal natural frequency ω_0, respectively. Then, (3.9) can be linearized about the nominal frequency ω_0 as

$$\delta\omega_s(t) = k_\omega k_\theta f(t) * \frac{1}{\zeta(t)\omega_0}\left[\delta\omega_n(t) - \delta\omega_s(t)\right]. \tag{3.10}$$

Moreover, letting ζ_0 be the nominal value of $\zeta(t)$, the system described by (3.25) can

be further approximated by the linear time-invariant system

$$\delta\omega_s(t) = k_\omega k_\theta f(t) * \frac{1}{\zeta_0\omega_0}\left[\delta\omega_n(t) - \delta\omega_s(t)\right]. \tag{3.11}$$

Taking the Laplace transform of both sides of this equation, it follows that

$$\Delta\Omega_s(s) = \frac{k_\omega k_\theta}{\zeta_0\omega_0}F(s)\left[\Delta\Omega_n(s) - \Delta\Omega_s(s)\right], \tag{3.12}$$

where $\Delta\Omega_n(s)$ and $\Delta\Omega_s(s)$ are the Laplace transforms of $\delta\omega_n(t)$ and $\delta\omega_s(t)$, respectively. Thus, the transfer function from $\delta\omega_n(t)$ to $\delta\omega_s(t)$ is

$$\frac{\Delta\Omega_s(s)}{\Delta\Omega_n(s)} = \frac{kF(s)}{1 + kF(s)}, \tag{3.13}$$

where $k = (k_\omega k_\theta)/(\zeta_0\omega_0)$.

The block diagram of (3.13) is shown in Figure 3.1. Having obtained this simplified model, the performance of the RST1 can be analyzed using standard linear control system analysis methods. It should be noted that this linear approximation is quite accurate provided that

$$\frac{|\delta\omega_n(t) - \delta\omega_s(t)|}{\zeta_0\omega_0} \leq 1. \tag{3.14}$$

This inequality arises from the approximation $\arctan[x] \approx x$ around the origin. Clearly this approximation is only accurate around a small region, as the arctangent function is similar to the saturation function.

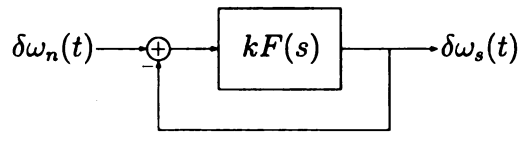

Figure 3.1. Linearized model of RTS1.

3.2.2 RTS2

Consider the resonance tuning system shown in Figure 2.14 and assume that PD is an exor type phase detector. Further assume that the excitation source $x(t)$ is in the form

$$x(t) = A_1(t)\cos\left[\omega_0 t + \theta_1(t)\right], \tag{3.15}$$

where $A_1(t) > 0$ is the amplitude, ω_0 is the angular frequency and $\theta_1(t)$ is the instantaneous phase of the input $x(t)$. The amplitude $A_1(t)$ and the phase $\theta_1(t)$ are also assumed to be slowly time-varying parameters. The instantaneous frequency $\omega_s(t)$ of the input $x(t)$ is defined as in (3.1).

Under these assumptions, the voltage $y(t)$ across the capacitor satisfies the differential equation (2.31). Since this equation is time varying, it is impossible to find the voltage $y(t)$ analytically. However, again using the frozen time approach, $\omega_c(t)$, $\omega_n(t)$, $\zeta(t)$, $A_1(t)$ and $\theta_1(t)$ can be treated as constant but unknown. Hence, the transfer function from $x(t)$ to $y(t)$ is

$$H(s) = \frac{\omega_c^2(t)}{s^2 + 2\zeta(t)\omega_n(t)s + \omega_c^2(t)}. \tag{3.16}$$

Thus, the voltage $y(t)$ can be expressed approximately as

$$y(t) = A_2(t)\cos\left[\omega_0 t + \theta_2(t)\right], \tag{3.17}$$

where $A_2(t) = |H[j\omega_s(t)]|A_1(t)$ and $\theta_2(t) = \theta_1(t) + \angle H[j\omega_s(t)]$. It then follows that

$$\theta_2(t) - \theta_1(t) = \angle H[j\omega_s(t)]. \tag{3.18}$$

Using this in (2.22), the output of the phase detector becomes

$$v(t) = f(t) * \varphi_e \left(\angle H[j\omega_s(t)] \right). \tag{3.19}$$

Since $-\pi < \angle H[j\omega_s(t)] \leq 0$, it follows from the phase comparator characteristic that

$$v(t) = -k_\theta f(t) * \left(\angle H[j\omega_s(t)] + \pi/2 \right), \tag{3.20}$$

where $k_\theta = 2V/\pi$ is the gain of the phase detector. Hence, using

$$\angle H[j\omega_s(t)] = -\arctan\left[\frac{2\zeta(t)\omega_n(t)\omega_s(t)}{\omega_c^2(t) - \omega_s^2(t)}\right] \tag{3.21}$$

in (3.20) yields

$$v(t) = k_\theta f(t) * \arctan\left[\frac{\omega_s^2(t) - \omega_c^2(t)}{2\zeta(t)\omega_n(t)\omega_s(t)}\right]. \tag{3.22}$$

Moreover, it follows from (2.29) that

$$v(t) = \frac{1}{k_\omega} \frac{\omega_c^2(t) - \omega_n^2(t)}{\omega_n^2(t)}. \tag{3.23}$$

Thus, combining (3.23) and (3.22) results in

$$\frac{\omega_c^2(t) - \omega_n^2(t)}{\omega_n^2(t)} = k_\omega k_\theta f(t) * \arctan\left[\frac{\omega_s^2(t) - \omega_c^2(t)}{2\zeta(t)\omega_n(t)\omega_s(t)}\right], \tag{3.24}$$

which describes the dynamics of the resonance tuning system.

Although several approximations are made to obtain (3.24), simulations indicate that this equation characterizes the operation of the resonance tuning system very accurately. However, since (3.24) is nonlinear and time-varying, it has limited value in design. Thus, this equation is linearized about the nominal frequency ω_0 to obtain a more tractable linear time-invariant model that facilitates both analysis and design.

Toward this end, let $\delta\omega_s(t) = \omega_s(t) - \omega_0$, $\delta\omega_n(t) = \omega_n(t) - \omega_0$ and $\delta\omega_c(t) = \omega_c(t) - \omega_0$ be the deviations of $\omega_s(t)$, $\omega_n(t)$ and $\omega_c(t)$ from the nominal natural frequency ω_0, respectively. Then, the Jacobian linearization of (3.24) about the nominal frequency ω_0 is

$$\delta\omega_c(t) - \delta\omega_n(t) = \frac{k_\omega k_\theta}{2\zeta(t)} f(t) * [\delta\omega_s(t) - \delta\omega_c(t)]. \tag{3.25}$$

Moreover, letting ζ_0 be the nominal value of $\zeta(t)$, the system in (3.25) can be further approximated by the linear time-invariant system

$$\delta\omega_c(t) - \delta\omega_n(t) = \frac{k_\omega k_\theta}{2\zeta_0} f(t) * [\delta\omega_s(t) - \delta\omega_c(t)]. \tag{3.26}$$

Finally, letting $k = k_\omega k_\theta/(2\zeta_0)$, the simplified linear time-invariant model of the resonance tuning system becomes

$$\delta\omega_c(t) - \delta\omega_n(t) = kf(t) * [\delta\omega_s(t) - \delta\omega_c(t)]. \tag{3.27}$$

Taking the Laplace transform of both sides of this equation yields

$$\Delta\Omega_c(s) - \Delta\Omega_n(s) = kF(s)\,[\Delta\Omega_s(s) - \Delta\Omega_c(s)]. \tag{3.28}$$

where $\Delta\Omega_s(s)$, $\Delta\Omega_n(s)$ and $\Delta\Omega_c(s)$ are the Laplace transforms of $\delta\omega_s(t)$, $\delta\omega_n(t)$ and $\delta\omega_c(t)$, respectively. Thus, it follows that

$$\Delta\Omega_c(s) = \frac{kF(s)}{1 + kF(s)}\Delta\Omega_s(s) + \frac{1}{1 + kF(s)}\Delta\Omega_n(s). \tag{3.29}$$

The block diagram of the system described by (3.29) is shown in Figure 3.2.

Having obtained this simplified model, the performance of RTS2 can be analyzed using standard linear control system analysis methods. As with RTS1, it should be

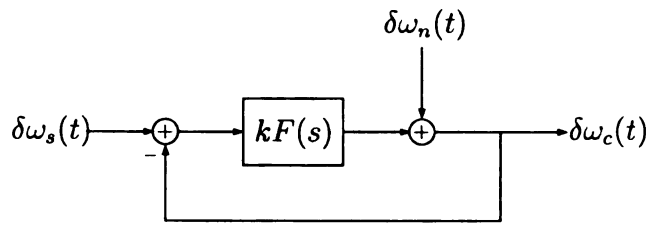

Figure 3.2. Simplified model of the resonance tuning system.

noted that this approximation is quite accurate provided that

$$\frac{|\delta\omega_s(t) - \delta\omega_c(t)|}{\zeta_0\omega_0} \leq 1. \tag{3.30}$$

3.2.3 RTS3

Consider the resonance tuning system shown in Figure 2.15 and assume that the phase detector is a multiplication type. Again, assume that the input $x(t)$ is in the form of (3.15). The output $y(t)$ satisfies the differential equation (2.33). As this equation is time varying, it is impossible to find $y(t)$ analytically, but again, with the frozen time approach the transfer function from $x(t)$ to $y(t)$ can be written as

$$H(s) = \frac{k_g\omega_n^2(t)}{s^2 + 2\zeta(t)\omega_n(t)s + \omega_c^2(t)}. \tag{3.31}$$

The output $y(t)$ can be approximated using its steady-state part as

$$y(t) = A_2(t)\cos\left[\omega_0 t + \theta_2(t)\right], \tag{3.32}$$

where $A_2(t) = |H[j\omega_s(t)]|A_1(t)$ and $\theta_2(t) = \theta_1(t) + \angle H[j\omega_s(t)]$. It then follows that

$$\theta_2(t) - \theta_1(t) = \angle H[j\omega_s(t)]. \tag{3.33}$$

Using this in (2.17) yields

$$v(t) = f(t) * \varphi_m \left(\angle H[j\omega_s(t)] \right). \tag{3.34}$$

Thus, the output of the phase detector becomes

$$v(t) = f(t) * \frac{A_1^2(t)}{2} |H[j\omega_s(t)]| \cos \left(\angle H[j\omega_s(t)] \right). \tag{3.35}$$

Since

$$|H[j\omega_s(t)]| \cos \left(\angle H[j\omega_s(t)] \right) = \mathrm{Re}\{H[j\omega_s(t)]\}, \tag{3.36}$$

the phase detector output can be rewritten as

$$v(t) = f(t) * \frac{A_1^2(t) k_g \omega_n^2(t) \left[\omega_c^2(t) - \omega_s^2(t) \right]}{2 \left(\left[\omega_c^2(t) - \omega_s^2(t) \right]^2 + \left[2\zeta(t)\omega_n(t)\omega_s(t) \right]^2 \right)}. \tag{3.37}$$

Next, solving (2.34) for $v(t)$ and substituting into (3.37), it follows that

$$\frac{\omega_c^2(t) - \omega_n^2(t)}{\omega_n^2(t)} = f(t) * \frac{k_w k_g A_1^2(t) \omega_n^2(t) \left[\omega_c^2(t) - \omega_s^2(t) \right]}{2 \left(\left[\omega_c^2(t) - \omega_s^2(t) \right]^2 + \left[2\zeta(t)\omega_n(t)\omega_s(t) \right]^2 \right)}, \tag{3.38}$$

which describes the dynamics of the resonance tuning system with a multiplication type phase detector.

Equation (3.38) is a nonlinear model of the resonance tuning system. Although simulations show that it represents the actual resonance tuning system very accurately, the nonlinear nature of this equation reduces its value from a design perspective. Therefore, this equation is linearized about the nominal angular frequency ω_0. For this purpose, let $\omega_s(t) = \omega_0 + \delta\omega_s(t)$, $\omega_c(t) = \omega_0 + \delta\omega_c(t)$ and $\omega_n(t) = \omega_0 + \delta\omega_n(t)$. Assume further that $\zeta(t)$ and $A_1(t)$ are equal to their respective nominal values ζ_0

and A_0. Then, linearization yields

$$\delta\omega_c(t) - \delta\omega_n(t) = f(t) * \frac{k_\omega k_\theta}{2\zeta_0} \left[\delta\omega_s(t) - \delta\omega_c(t)\right], \tag{3.39}$$

where $k_\theta = -k_g A_0^2/(4\zeta_0)$. Finally, letting $k = k_\omega k_\theta/(2\zeta_0)$, the simplified linear time-invariant model of the resonance tuning system becomes

$$\delta\omega_c(t) - \delta\omega_n(t) = kf(t) * \left[\delta\omega_s(t) - \delta\omega_c(t)\right]. \tag{3.40}$$

Again, it should be noted that this approximation is quite accurate provided that

$$\frac{|\delta\omega_s(t) - \delta\omega_c(t)|}{\zeta_0\omega_0} \leq 1. \tag{3.41}$$

The block diagram of the system described by (3.40) is shown in Figure 3.2. It is evident from this figure that the lowpass filter plays an important role in the resonance tuning system.

3.3 Stability

3.3.1 Linear Models

From the linear models of RTS1 (3.11), RTS2 (3.27) and RTS3 (3.40), it follows that these systems are stable if all the roots of the characteristic equation $1+kF(s) = 0$ have negative real parts. Under this condition, it can be concluded that the original nonlinear and time-varying resonance tuning systems given in Figure 2.12, Figure 2.14 and Figure 2.15 are also stable provided that the rate of variations of the slowly varying parameters are sufficiently small [30]. However, for completeness, nonlinear stability analysis is required.

3.3.2 Nonlinear Models

In this section, the stability properties of the resonance tuning systems are studied.

Saturation Like Nonlinearity

In [20], analysis of RTS3 with an exor phase detector is provided. From this analysis, it can be seen that the nonlinear model of RTS3 is identical to the nonlinear model of RTS2, which is given in this thesis by (3.24). In this model, the nonlinearity has the nature of an arctangent function. As seen in Figure 3.3, the arctangent function represented by the solid line is very similar to the saturation function represented by the dashed line. Due to this similarity, a theorem pertaining to systems

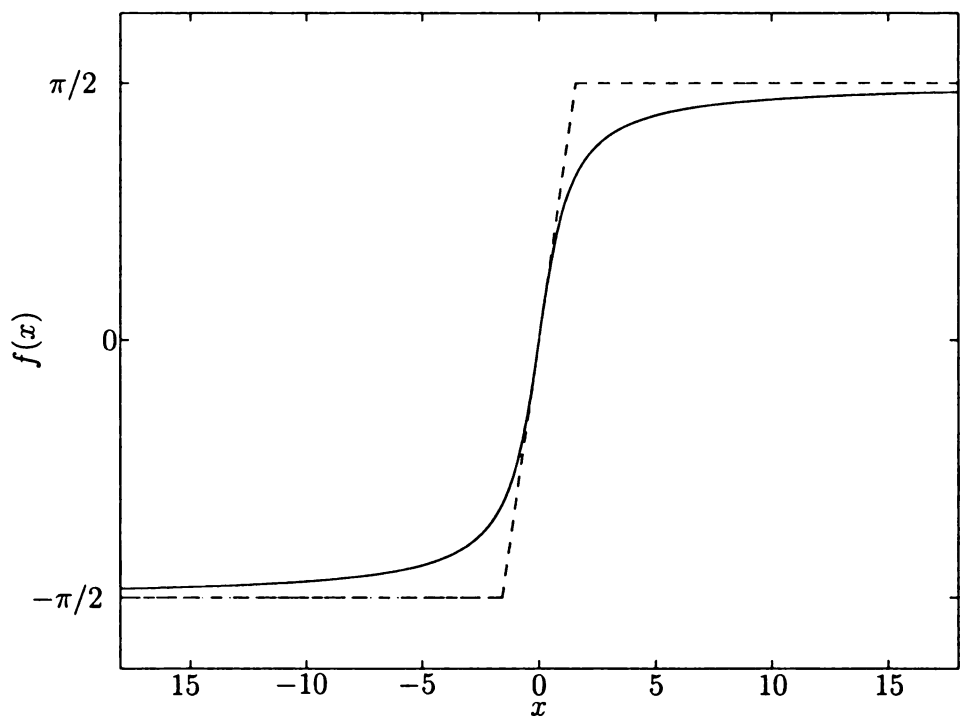

Figure 3.3. Plot of arctangent and saturation functions.

with a saturation nonlinearity in [17] is adapted to the arctangent nonlinearity in this work. For this purpose, first let the output $\omega_c(t)$ equal its nominal value ω_0 plus some perturbation term $\delta\omega_c(t)$. Also, let $\omega_s(t)$ and $\omega_n(t)$ equal the nominal value ω_0 and $\zeta(t) = \zeta_0$. Thus (3.24) becomes

$$\frac{\delta\omega_c^2(t) + 2\delta\omega_c(t)\omega_0}{\omega_0^2} = k_\omega k_\theta f(t) * \arctan\left[\frac{-\omega_c^2(t) - 2\delta\omega_c\omega_0}{2\zeta_0\omega_0^2}\right]. \tag{3.42}$$

Next, with the change of variable

$$z(t) = \frac{\delta\omega_c^2(t) + 2\delta\omega_c(t)\omega_0}{\omega_0^2}, \tag{3.43}$$

equation (3.42) becomes

$$z(t) = k_\omega k_\theta f(t) * \arctan\left[-\frac{1}{2\zeta_0}z(t)\right]. \tag{3.44}$$

Letting {A,B,C,0} be a minimal realization of $k_\omega k_\theta F(s)$, where $A \in \mathbb{R}^{n\times n}$, $B \in \mathbb{R}^{n\times 1}$ and $C \in \mathbb{R}^{1\times n}$ this system can be represented by the state equations

$$\begin{aligned} \dot{x}(t) &= Ax(t) + B\varphi(u(t)) \\ z(t) &= Cx(t) \\ u(t) &= Kx(t), \end{aligned} \tag{3.45}$$

where where $K = -\frac{1}{2\zeta_0}C$ and

$$\varphi\left[u(t)\right] = \arctan[u(t)], \tag{3.46}$$

Using the model (3.45), a theorem is provided below which states that, under very mild conditions, the origin $x = 0$ is the only equilibrium point of this system.

Theorem 3.1 *Consider the system (3.45), and assume that A has no eigenvalues with positive real parts. The origin x=0 is the only equilibrium point of this system if* $A + BK$ *is Hurwitz.*

Proof: By definition, any point $x \in \mathbb{R}^n$ is the equilibrium point of (3.45) if

$$Ax + B\varphi(Kx) = 0, \tag{3.47}$$

or, equivalently,

$$(A + BK)x + B[\varphi(Kx) - Kx] = 0. \tag{3.48}$$

Since $A + BK$ is nonsingular, it follows that

$$x + (A + BK)^{-1}B[\varphi(Kx) - Kx] = 0. \tag{3.49}$$

Premultiplying both sides of this equation by K, we obtain

$$[1 - K(A + BK)^{-1}B]Kx + K(A + BK)^{-1}B\varphi(Kx) = 0. \tag{3.50}$$

If $K(A+BK)^{-1}B = 0$, then this equation implies that $Kx = 0$, and in turn, equation (3.49) implies that $x = 0$. If, on the other hand, $K(A + BK)^{-1}B = 1$, then equation (3.50) implies that $Kx = 0$, and then, equation (3.49) implies that $x = 0$. Hence, assume that $K(A + BK)^{-1}B \neq 0$ and $K(A + B_2K)^{-1}B \neq 1$, then we claim that

$$K(A + BK)^{-1}B < 1. \tag{3.51}$$

To see this, note that

$$
\begin{aligned}
1 - K(A+BK)^{-1}B &= \det[I - (A+BK)^{-1}BK] \\
&= \det[(A+BK)^{-1}]\det(A) \geq 0,
\end{aligned}
\tag{3.52}
$$

and by assumption $K(A+BK)^{-1}B \neq 1$. Thus, under the above assumptions, it follows from (3.51) that either

$$
\frac{K(A+BK)^{-1}B - 1}{K(A+BK)^{-1}B} < 0, \tag{3.53}
$$

or

$$
\frac{K(A+BK)^{-1}B - 1}{K(A+BK)^{-1}B_2} > 1. \tag{3.54}
$$

Hence, rewriting (3.50) as

$$
\varphi(Kx) = \frac{K(A+BK)^{-1}B - 1}{K(A+BK)^{-1}B} Kx, \tag{3.55}
$$

we see that x satisfies this equation only when $Kx = 0$. Hence, once again equation (3.49) implies that $x = 0$, and this completes the proof. □

Note that since standard control system design requires $Re(\lambda) \leq 0$, the first condition of theorem (3.45) is generally satisfied. Also note that the system (3.45) may have either one isolated equilibrium (the origin), or three isolated equilibria (one being the origin). Moreover, since the Jacobian linearization of (3.45) around the origin is

$$
\delta\dot{x} = (A+BK)\delta x, \tag{3.56}
$$

it follows from the Lyapunov's indirect method [30] that if $A+BK$ is Hurwitz, then the origin is asymptotically stable. Combining this result with that of Theorem 3.1, we obtain the following

Corollary 3.1 *Under the assumptions of Theorem 3.1, the origin $x = 0$ is the unique asymptotically stable equilibrium of the closed-loop system (3.45).*

Proof: The proof of this corollary follows from the Lyapunov's indirect method and Theorem 3.1. □

Next, assuming A is Hurwitz, we show that the solution of (3.45) remains bounded for all time.

Theorem 3.2 *Consider the system (3.45), and assume that A is Hurwitz. Then, $x(t)$ is bounded for all time, i.e., there exists an $m > 0$ such that $\|x(t)\| \leq m$ for all $t \geq 0$.*

Proof: The solution of (3.45) starting from $x(0)$ satisfies

$$x(t) = \exp(At)x(0) + \int_0^t \exp[A(t-\tau)]B\varphi[Kx(\tau)]d\tau. \tag{3.57}$$

Hence,

$$\|x(t)\| \leq \|\exp(At)x(0)\| + \|\int_0^t \exp[A(t-\tau)]B\varphi[Kx(\tau)]d\tau\|. \tag{3.58}$$

Then, it follows that

$$\begin{aligned} \|x(t)\| &\leq \exp(-\nu t)\|x(0)\| + \frac{k_\omega k_\theta \pi}{2\nu}[1 - \exp(-\nu t)]\|B\| \\ &\leq \|x(0)\| + \frac{k_\omega k_\theta \pi}{2\nu}\|B\|, \end{aligned} \tag{3.59}$$

where ν is the real part of the rightmost eigenvalue of A. Thus, letting

$$m = \|x(0)\| + \frac{k_\omega k_\theta \pi}{2\nu}\|B\|, \tag{3.60}$$

we see that $\|x(t)\| \leq m$ for all $t \geq 0$.

□

Circle Criterion

The previous discussion requires A to be Hurwitz for global asymptotic stability. However, this may not be the case as $F(s)$ can contain an integrator. For this purpose, we consider the circle criterion to show asymptotic stability with a finite domain. To use the circle criterion, we must first represent the system as a feedback connection of a linear system and nonlinear element, as shown in Figure 3.4. Here, $G(s)$ is the linear system and $\Psi[u(t)]$ is the nonlinear element.

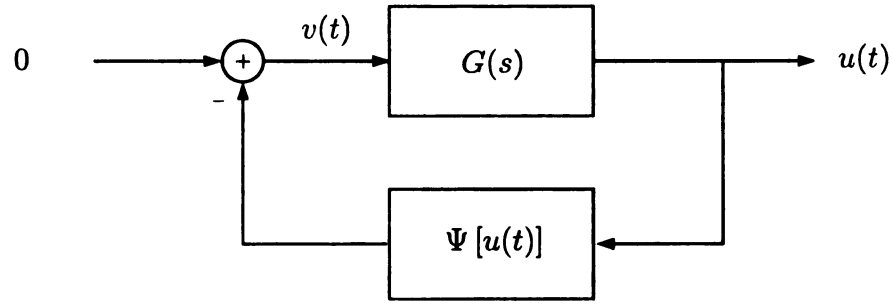

Figure 3.4. Feedback connection of linear system and nonlinear element.

To illustrate this, first consider the nonlinear model of RTS2 and RST3 with an exor phase detector given by (3.24). As seen earlier, this model can be represented by the state equations (3.45). In order to transform this model into the form of

Figure 3.4, let $v(t) = \varphi[u(t)]$ and $\Psi[u(t)] = -\varphi[u(t)]$. Hence,

$$G(s) = K(sI - A)^{-1}B. \tag{3.61}$$

Clearly, $\Psi[u(t)] \in [0, \frac{1}{2\zeta_0}]$. However, since $G(s)$ is not assumed Hurwitz, in order to apply the circle criterion, the nonlinearity must remain within the sector $[\alpha, \beta]$, where $0 < \alpha < \beta$. The arctangent function will eventually leave this sector no matter how small the value of α is, as seen in Figure 3.5. For this reason, we can only conclude absolute stability with a finite domain [30]. Using the circle criterion, the

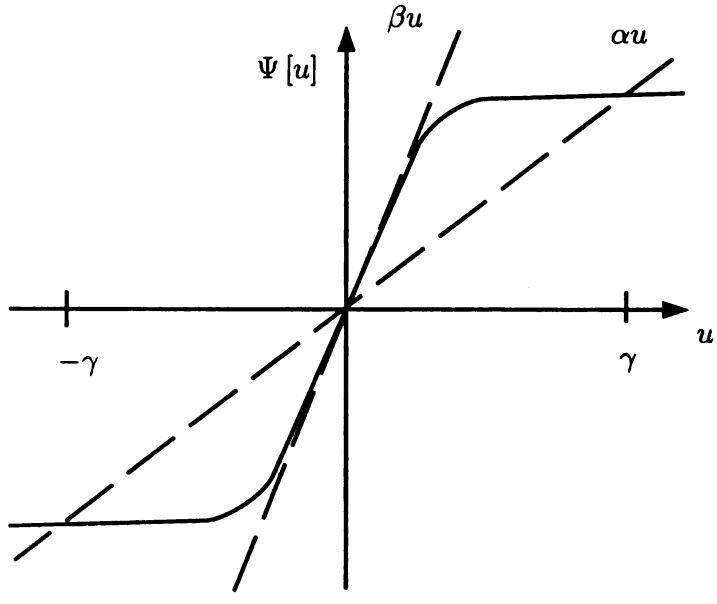

Figure 3.5. Sector bounded nonlinearity of RTS2 and RTS3 with exor PD.

following theorem is stated.

Theorem 3.3 *The system in Figure 3.4 is absolutely stable with a finite domain if* $0 < \alpha < \beta$ *and the Nyquist plot of* $G(j\omega)$ *does not enter the disk* $D(\alpha, \beta)$.

Proof: To satisfy theorem 3.3,

$$Re\left[\frac{1+\beta G(j\omega)}{1+\alpha G(j\omega)}\right] > 0. \tag{3.62}$$

From equation 3.61,

$$G(s) = \frac{1}{2\zeta_0} C(sI - A)^{-1}B, \tag{3.63}$$

which can be rewritten as

$$G(s) = \frac{1}{2\zeta_0} k_\omega k_\theta F(s). \tag{3.64}$$

Hence,

$$Re\left[\frac{1+\beta k F(j\omega)}{1+\alpha k F(j\omega)}\right] > 0, \tag{3.65}$$

where $k = \frac{1}{2\zeta_0} k_\omega k_\theta$. The remainder of the proof then clearly follows from the proof of the circle criterion in [30], which uses the fact that that the storage function

$$V(x) = \frac{1}{2} x^T P x \tag{3.66}$$

for the linear dynamical system satisfies the Kalman-Yakubovich-Popov equations.

□

Using a multiplication phase detector, and following the same process as before, the nonlinear model of RST3 (3.38) can be written as

$$\frac{\delta\omega_c^2(t) + 2\delta\omega_c(t)\omega_0}{\omega_0^2} = k_\omega k_g A_1^2 \omega_0^2 f(t) * \frac{\delta\omega_c^2(t) + 2\delta\omega_c(t)\omega_0}{\left(\delta\omega_c^2(t) + 2\delta\omega_c(t)\omega_0\right)^2 + \left(2\zeta_0\omega_0\right)^2}. \tag{3.67}$$

With the change of variables

$$z(t) = \delta\omega_c^2(t) + 2\delta\omega_c(t)\omega_0, \tag{3.68}$$

this equation can be written

$$z(t) = f(t) * K\frac{z(t)}{z^2(t) + (2\zeta_0\omega_0^2)}. \tag{3.69}$$

Again using the circle criterion with the requirement that $\alpha > 0$, it follows that (3.69) will only remain sector bounded in a finite domain. This can be seen from Figure 3.6. Hence, the same method as above can be applied to show stability with a finite domain.

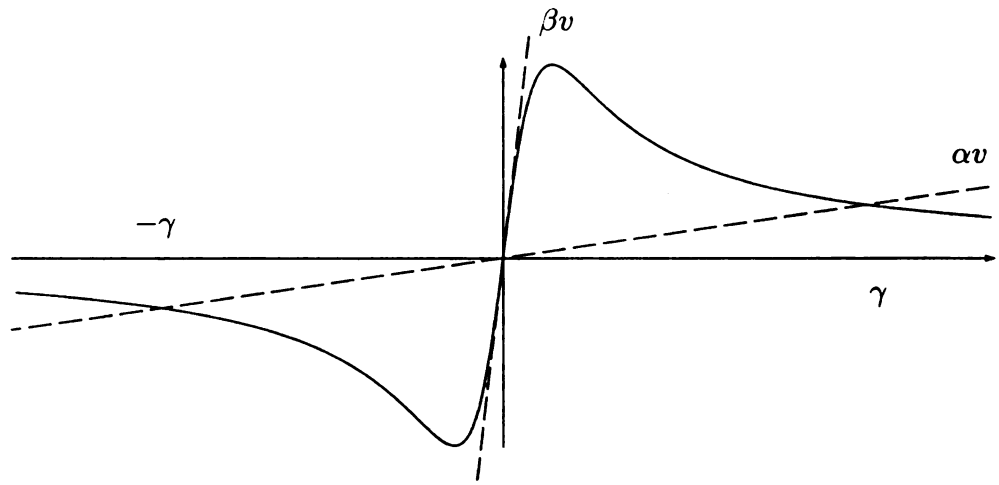

Figure 3.6. Sector bounded nonlinearity of RTS3 with multiplication PD.

Finally, consider the nonlinear model of RTS1 given by (3.11). Let the output $\omega_s(t)$ equal its nominal value ω_0 plus some perturbation term $\delta\omega_s$. Also, let $\omega_n(t)$

equal the nominal value ω_0 and $\zeta(t) = \zeta_0$. Thus (3.24) becomes

$$\delta\omega_s = k_\omega k_\theta f(t) * \arctan\left[-\frac{\delta\omega_s\,(\delta\omega_s - 2\omega_0)}{2\zeta_0\omega_0\,(\delta\omega_s + \omega_0)}\right]. \tag{3.70}$$

It should be noted that the nonlinearity of this equation is not bounded by a sector with an upper bound equal to the slope of the arctangent function, as is the case with RTS2 and RTS3. Instead, as $\delta\omega_s$ moves away from the origin in the negative direction, this nonlinearity will always start outside the sector. However, circle criterion may still be applied to this case by simply increasing the value of β to include this portion of the nonlinearity in the sector. For illustrative purposes, an exaggerated view of this nonlinearity is shown in Figure 3.7.

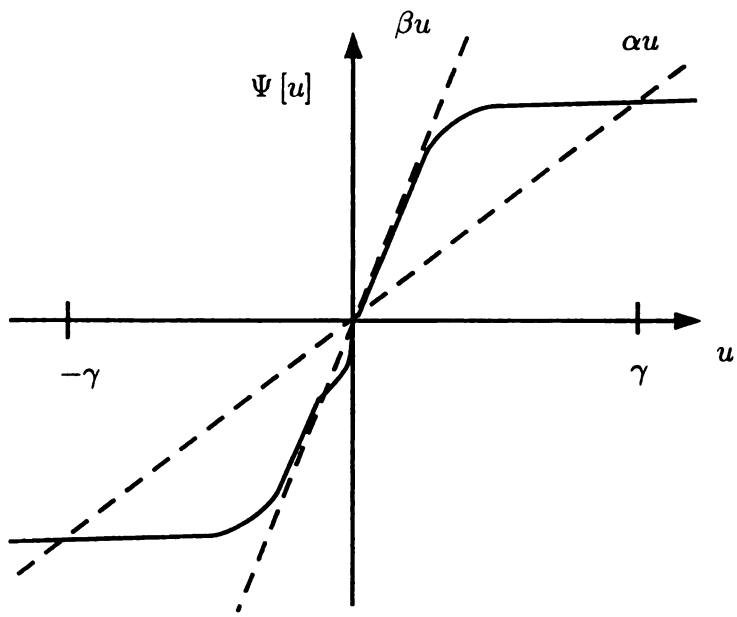

Figure 3.7. RTS1 nonlinearity crossing the sector bound near the origin.

CHAPTER 4

Design

In this chapter, the design problem formulated above is considered and some guidelines for designing the resonance tuning system are provided. Using these guidelines, the actual resonance tuning systems, their nonlinear time-varying models and their simplified linear time-invariant models are simulated using the parameters of the previously discussed applications. These simulation results illustrate the performance of the resonance tuning systems and verify the accuracy of the proposed simplified models. All simulations are carried out in MATLAB/Simulink.

4.1 Design

Based on the developed simplified linear time-invariant models, the resonance tuning systems can be designed using standard control system design methods. For RTS1, the goal of the design is to find the "controller" $F(s)$ so that the "output" $\delta\omega_s(t)$ tracks the "reference" $\delta\omega_n(t)$ satisfactorily. For RTS2 and RTS3, the goal of the design is to find the "controller" $F(s)$ so that the "output" $\delta\omega_c(t)$ tracks the "reference" $\delta\omega_s(t)$ satisfactorily.

In designing the resonance tuning system, the following guidelines should be taken into consideration. As a direct consequence of the internal model principle [29], to achieve perfect asymptotic reference tracking the filter $F(s)$ must contain the model of the reference ($\delta\omega_n(t)$ for RTS1 or $\delta\omega_s(t)$ for RTS2 and RTS3). Similarly, the filter $F(s)$ must contain the model of the disturbance $\delta\omega_n(t)$ to achieve perfect

asymptotic disturbance rejection (RTS2 and RTS3). In particular, for the output to asymptotically track any step change in the reference and asymptotically reject any step change in the disturbance, the filter $F(s)$ must contain at least one integrator. Moreover, the bandwidth of the lowpass filter $F(s)$ should be sufficiently small to filter out the higher order harmonics at the output of the phase comparator. In addition, the bandwidth of $kF(s)/[1 + kF(s)]$ should be sufficiently large for good reference tracking whereas the gain of $1/[1 + kF(s)]$ should be sufficiently small for good disturbance rejection.

In most practical applications, a first order filter of the form

$$F(s) = \frac{\beta}{s}, \tag{4.1}$$

where β is a design parameter, usually gives adequate results. With this filter, the settling time for $\delta\omega_s(t)$ in RTS1 or $\delta\omega_c(t)$ in RTS2 and RTS3 calculated from the linearized model is $\tau = 4/(k\beta)$. If the desired performance is not achievable by a first order filter, a second order filter of the form

$$F(s) = \frac{\beta}{s(s+\alpha)}, \tag{4.2}$$

where α and β are design parameters, may be used. For this case, the settling time for $\delta\omega_s(t)$ or $\delta\omega_c(t)$ calculated from the linearized model is $\tau = 8/\alpha$ provided that $\alpha^2 \leq 4k\beta$.

These well established linear system design methods are generally suitable. However, in certain applications, for instance when (3.14), (3.30) and (3.41) are not satisfied, the linear system will not accurately represent the resonance tuning system. In this instance, the linear system is still valuable in that it acts as a starting point for the design process, however, some guidelines pertaining to the nonlinear system are

helpful. Currently, more research is required to provide definite methods for determining parameters such as rise time and settling time for the nonlinear models. However, using the theorems provided in Section 3.3, the resonance tuning systems can be easily designed so that stability is guaranteed even in the absence of an accurate linear model.

4.2 Simulation

4.2.1 RTS1

In this section, the original RTS1, its nonlinear time-varying model and its simplified linear time-invariant model are simulated. These simulation results illustrate the performance of RTS1 and verify the accuracy of the proposed simplified model.

Assume that the nominal values of the parameters $R(t)$, $L(t)$ and $C(t)$ of this system are $R_0 = 0.25\ \Omega$, $L_0 = 0.1$ H and $C_0 = 10\ \mu$F, respectively, so that the nominal values of $\omega_n(t)$, $\zeta(t)$ and $Q(t)$ are $\omega_0 = 1000$ rad/s, $\zeta_0 = 0.00125$ and $Q_0 = 400$. Assume further that $V = 2.5$ V so that $k_\theta = 1.592$ V/rad. Let $k_\omega = 50\ \text{V}^{-1}$ and assume the center frequency of the VCO is $\omega_0 = 1000$ rad/s. Hence, the system is tuned to its resonant frequency. However, as before assume the value of $C(t)$ decreases by 1 percent, so that the resonant frequency of the system becomes 1005.04 rad/s. For the second order filter

$$F(s) = \frac{0.7451}{s(s+20)}, \tag{4.3}$$

the response of the actual RTS1 shown in Figure 2.12, the nonlinear model (3.9) and the linear model (3.11) to this input step change is shown in Figure 4.1. In this figure the solid line is the response of the actual resonance tuning system, the dashed line is the response of the nonlinear model, and the dashdot line is the response of the linear model.

It is evident from this figure that RTS1 is working satisfactorily and that the two simplified models are reasonably accurate approximations of the actual RTS1 system. However, to demonstrate the range of this resonance tuning system, a second simulation is considered. Assume the same parameters as before, but now with a 10 percent decrease in $C(t)$, so that the resonant frequency of the system becomes 1054.1 rad/s. The response is shown in Figure. 4.2. From this figure, it is clear that RTS1 successfully tunes $\omega_s(t)$ to $\omega_n(t)$. However, it is also clear that the linear time-invariant model is no longer an accurate representation of the actual RTS1. This is due to the fact that (3.14) is not satisfied.

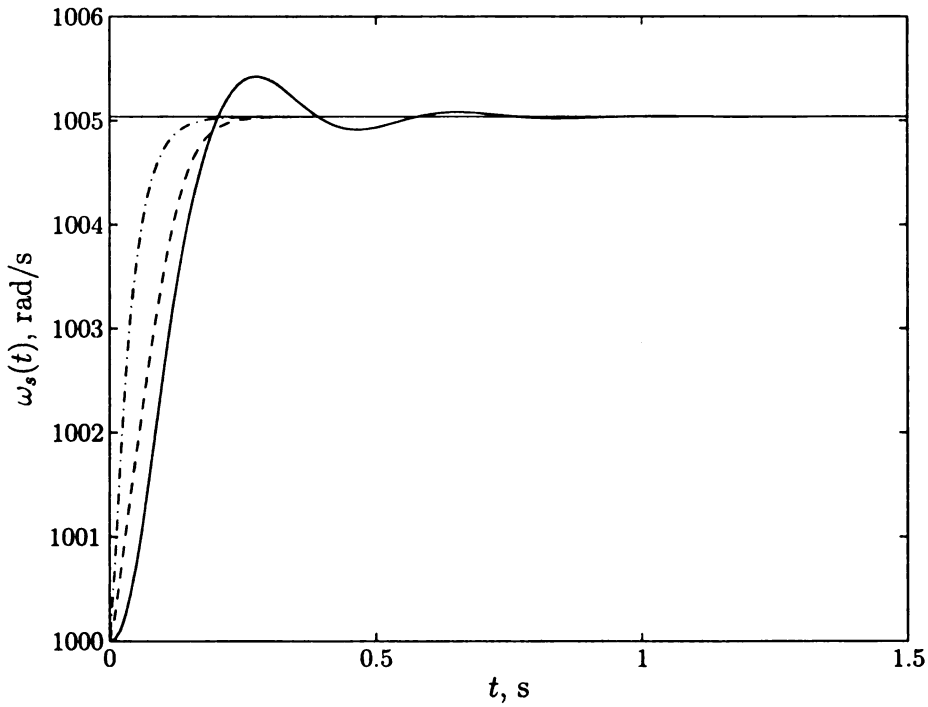

Figure 4.1. Simulation results of RTS1 with $\omega_n = 1005.04$.

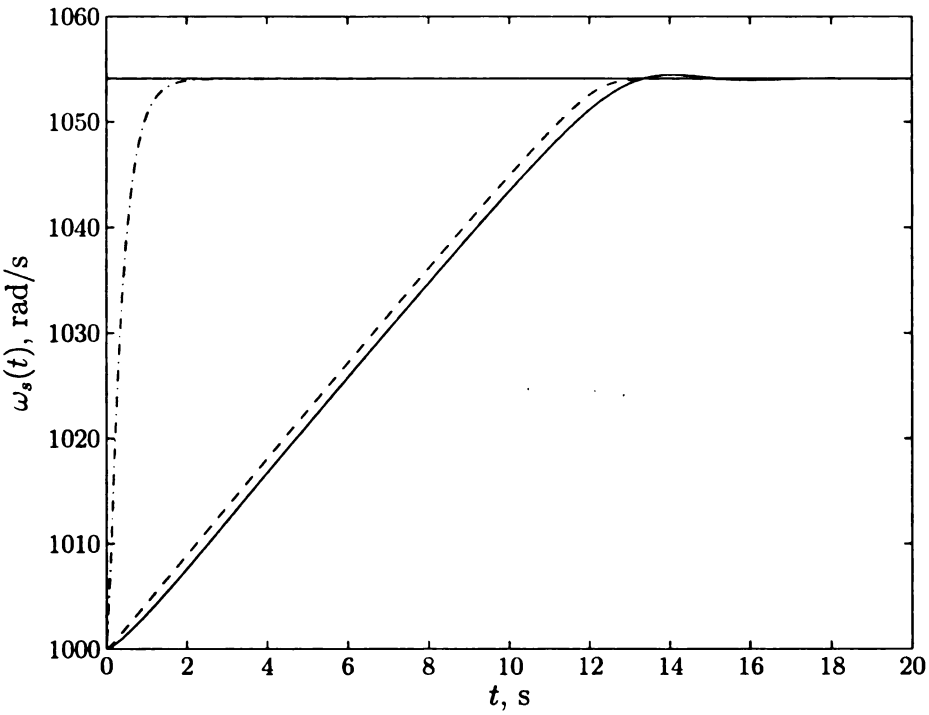

Figure 4.2. Simulation results of RTS1 with $\omega_n = 1054.1$.

4.2.2 RTS2

In this section, the original RTS2, its nonlinear time-varying model and its simplified linear time-invariant model are simulated. These simulation results illustrate the performance of RTS2 and verify the accuracy of the proposed simplified model.

Assume that the nominal values of $R(t)$, $L(t)$ and $C(t)$ are $R_0 = 0.5\ \Omega$, $L_0 = 0.01$ H and $C_0 = 0.0001$ F, respectively, so that the nominal values of $\omega_n(t)$, $\zeta(t)$ and $Q(t)$ are $\omega_0 = 1000$ rad/s, $\zeta_0 = 0.025$ and $Q_0 = 20$, respectively. Assume also that $V = 2.5$ V so that $k_\theta = 1.592$ V/rad and let $k_\omega = 0.1\ \text{V}^{-1}$. Assume further that $R(t) = R_0$, $L(t) = L_0$ for all t, but $C(t)$ varies with time as $C(t) = 1.000 \times 10^{-4}$ F for 0 s $\leq t <$ 2 s and 8.264×10^{-5} F for 2 s $\leq t$ so that the uncontrolled resonant frequency $\omega_n(t)$ of the resonator undergoes a step change from 1000 rad/s to 1100 rad/s. Finally, assume that the excitation frequency $\omega_s(t)$ also undergoes a step change at time $t = 4$ s from

1000 rad/s to 900 rad/s.

For each of the following filters

$$F(s) = \frac{2.827}{s+1}, \quad F(s) = \frac{1.571}{s}, \quad F(s) = \frac{62.832}{s(s+20)}, \tag{4.4}$$

the original resonance tuning system shown in Fig. 2.14, its approximate nonlinear time-varying model given in (3.24) and its simplified linear time-invariant model given in (3.27) are simulated. The simulation results for the resonant frequency $\omega_c(t)$ are shown in Figs. 4.3, 4.4 and 4.5, respectively. In each figure, the solid curve is for the exact system, the dashed curve is for the approximate system and the dashdot curve is for the simplified system. The uncontrolled resonant frequency $\omega_n(t)$ and driving frequency $\omega_s(t)$ are also shown in each of these figures by the solid curves for comparison. These figures indicate that both the approximate nonlinear time-varying model and simplified linear time invariant model predict the behavior of exact system quite accurately.

Since the first filter does not contain an integrator, the error between the resonant frequency and driving frequency in the steady-state is not zero as predicted by the previous analysis. This error, on the other hand, is practically zero for the second and third filters as expected since they both contain an integrator. Note also that since the second order filter has better selectivity compared to the other two, its performance in the steady-state is superior to those of the first order filters.

These results show that the developed simplified model predicts the performance of the resonant tuning system quite accurately. Therefore, the developed simplified model can be used to facilitate both analysis and design of the resonance tuning system.

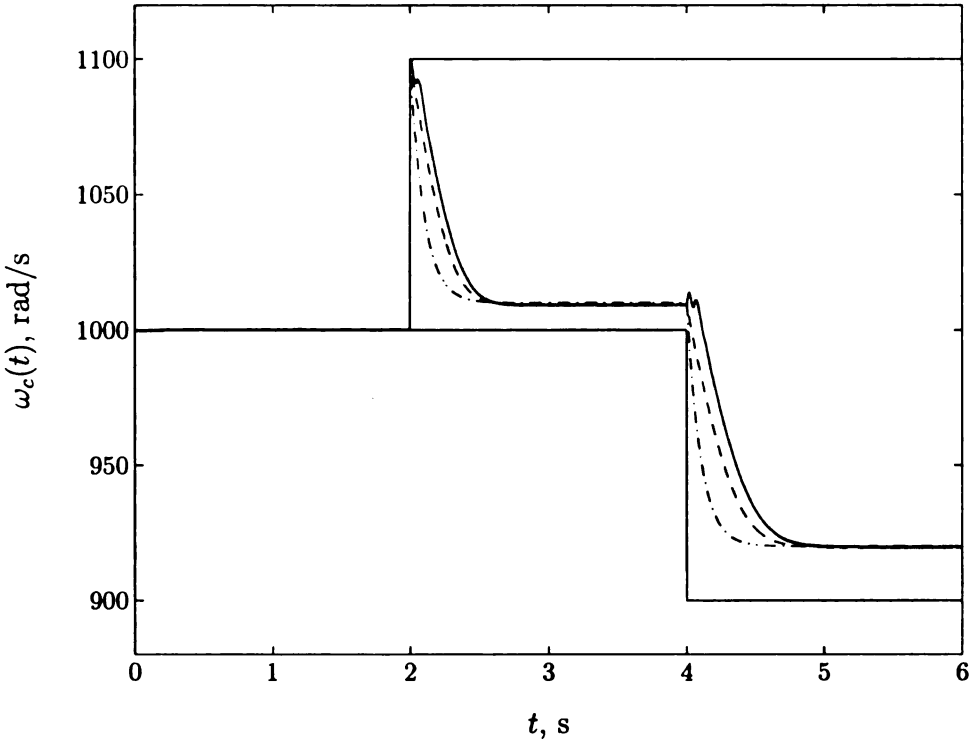

Figure 4.3. Simulation results with $F(s) = 2.827/(s+1)$.

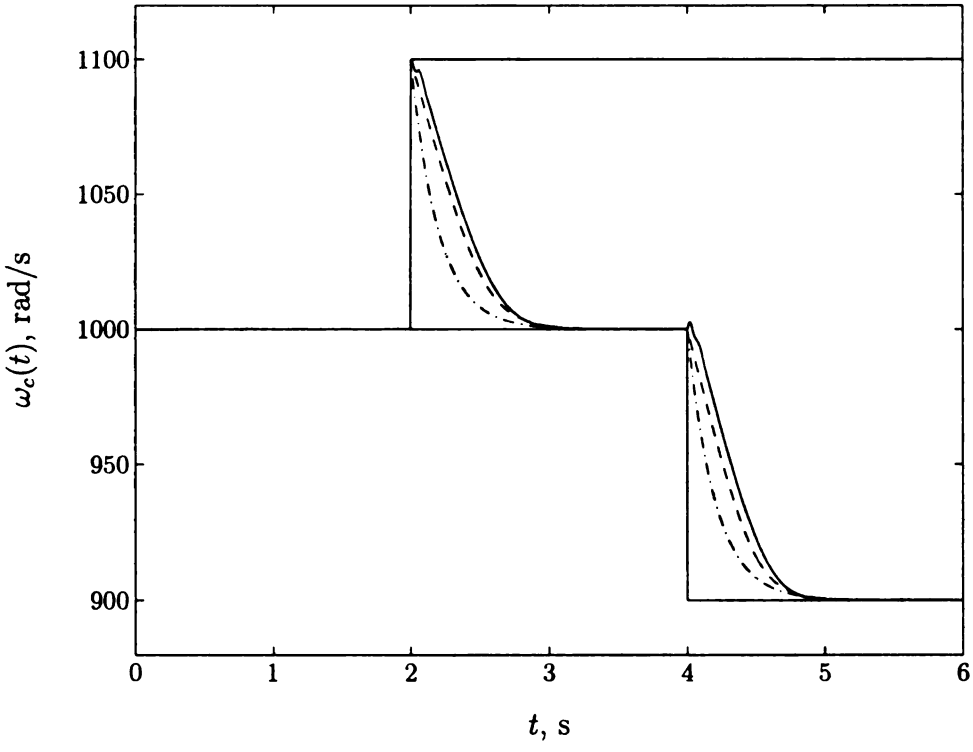

Figure 4.4. Simulation results with $F(s) = 1.571/s$.

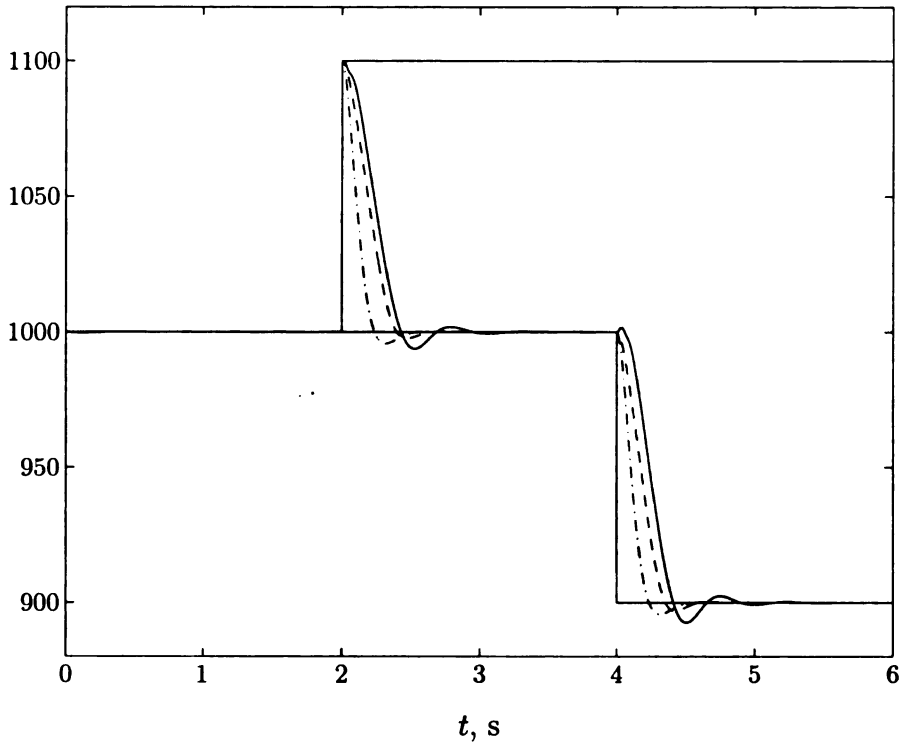

Figure 4.5. Simulation results with $F(s) = 62.832/[s(s + 20)]$.

4.2.3 RTS3

In this section, the developed analysis and design methods of RTS3 are applied to two examples. First, a vibrational gyroscope example from [6] is considered. Assume that the parameters of this system are $\omega_n(t) = 63881.1$ rad/s, $\zeta(t) = 0.0005$, $k_g = 0.0666$. Moreover, assume $\omega_s(t) = 65973.4$ rad/s and $A_1(t) = 1$. In the simulations below, the feedback gain k_f was selected as $k_f = 100$, the nominal frequency ω_0 was taken as $\omega_0 = 65973.4$ rad/s and the logic voltage V was chosen as $V = 2.5$ V.

The first simulation of RTS3 uses a multiplication phase detector with the first order low-pass filter

$$F(s) = -\frac{0.05}{s}, \tag{4.5}$$

The results of this simulation are shown in Figure 4.6. Here, the solid curve is for the actual system shown in Figure 2.15 and the dotted curve is for the nonlinear

time-varying model (3.38). The instantaneous input frequency $\omega_s(t)$ is also shown by the solid horizontal line for convenience.

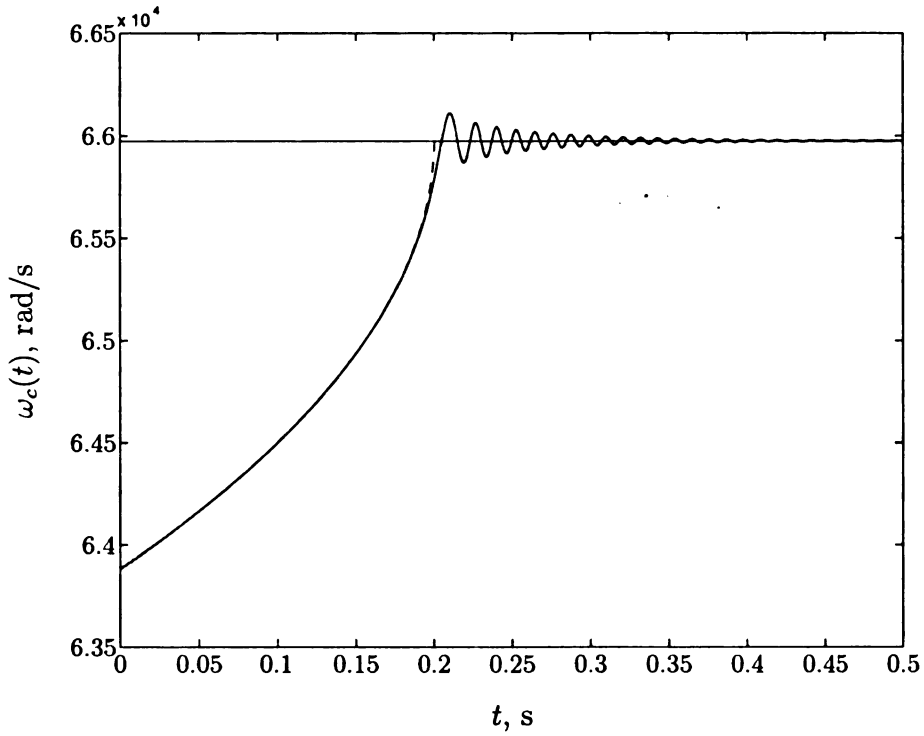

Figure 4.6. Simulation results of RTS3 for vibrational gyroscope example.

It should be noted that while the nonlinear model closely approximates the actual system, the corresponding linear model is quite different, and thus not shown in Figure 4.6. This is due to the fact that the deviation of $\omega_c(t)$ from the nominal frequency ω_0 is quite large initially. In other words, the system in [6] does not satisfy condition (3.41), and the nonlinearity in (3.38) behaves like saturation due to the extremely small damping ratio. This discrepancy reduces the values of the developed linear time invariant models since their predictions are no longer accurate. Therefore, unless the system is altered to satisfy (3.41), a different design strategy based on the developed nonlinear time varying models should be used. However, it should also be

pointed out that the developed linear model still provides some value in that it acts as starting point in the design process.

In order to illustrate the accuracy of the developed linear time invariant model when (3.41) is satisfied, a second example is considered. This simulation considers a hypothetical lightly damped second order system. The parameters of the resonance tuning system are as follows: $\omega_n(t) = 1000$ rad/s, $\zeta(t) = 0.05$, $k_g = 1$, $\omega_s(t) = 1050$ rad/s, $A_1(t) = 1$, $k_f = 0.5$, $\omega_0 = 1000$ rad/s and the phase detector is a multiplication type with second order filter

$$F(s) = \frac{10}{s\,(s+20)}. \tag{4.6}$$

The results of this simulation are shown in Figure 4.7. Here, the solid, dashed and dashdot curves are for the actual system shown in Figure 2.15, the nonlinear time-varying model (3.38) and the simplified linear time-invariant model (3.40), respectively. Again, the instantaneous input frequency $\omega_s(t)$ is shown by the solid horizontal line for convenience.

It is evident from Figure 4.7 that the developed models accurately predict the performance of the actual system, which was expected as (5.10) is satisfied in this generic example. Hence, the developed model can be used for both analysis and design of the resonance tuning system.

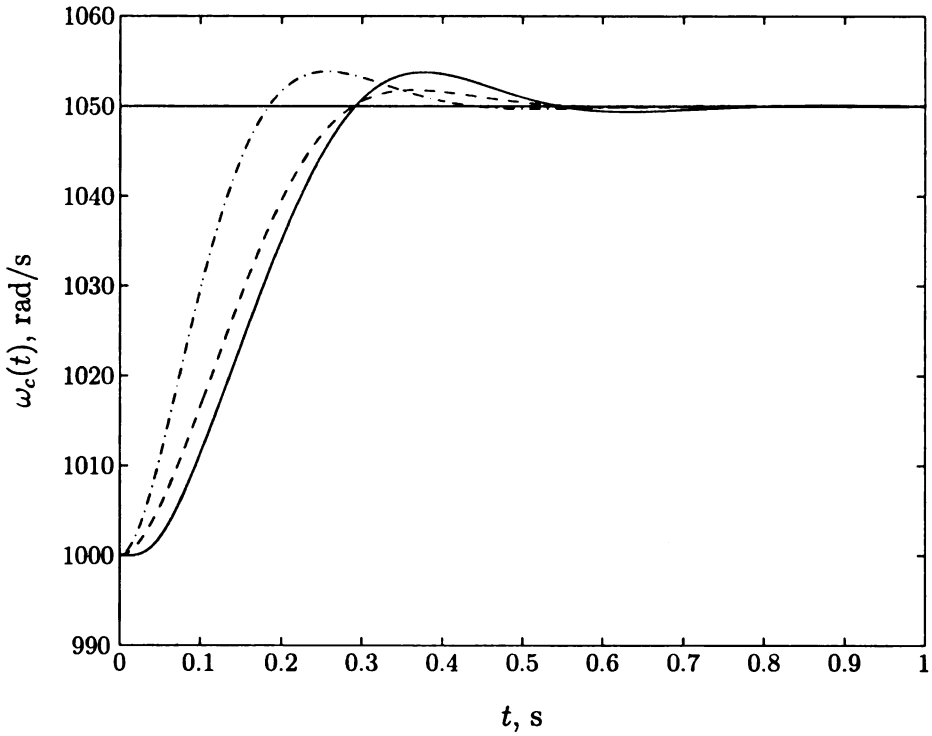

Figure 4.7. Simulation results of RTS3 with $F(s) = \frac{10}{s(s+20)}$.

CHAPTER 5

Extension - Adaptively Enhanced PLL

5.1 Introduction

The following presents an extended use of RTS2 and RTS3, in which these resonance tuning systems can be combined with a standard PLL to enhance the performance of the standard PLL. Much of the derivation behind the equations has been omitted as it is similar to the analysis presented earlier in this thesis. Initial results of the adaptively enhanced PLL are promising, however, more research on this topic still needs to be carried out.

5.2 Modeling

In this section, a model of the adaptively enhanced PLL is presented. This model can be seen in Figure 5.1. Here the input to the system is $x(t)$ and the output is $y(t)$. A standard PLL is represented by the components within the dashed box, where PC is a phase comparator, $F(s)$ is a lowpass filter and VCO is a voltage controlled oscillator. FE is a frequency estimator system that provides an estimate, $\omega_e(t)$, of the instantaneous frequency of $x(t)$ to the VCO. The purpose of the frequency estimator is to provide the voltage controlled oscillator (VCO) of the PLL with an appropriate free running angular frequency $\omega_e(t)$ that closely matches the frequency of the input.

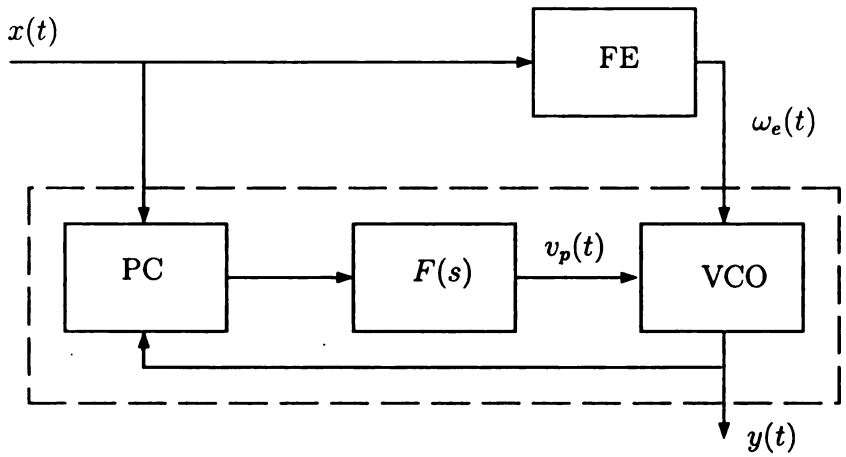

Figure 5.1. Model of the enhanced PLL system.

For this task, a method similar to that of RTS2 is used. In this method, the resonant frequency of a lightly damped second order system is changed using proportional feedback and the feedback gain is adaptively adjusted to tune the resonant frequency of the resulting closed loop system to its excitation frequency. Hence, at steady state, the resonant frequency of this closed loop system acts as an estimate of the excitation frequency.

A block diagram of the frequency estimator system is shown in Figure 5.2. In this figure, $H(s)$ is the transfer function of the lightly damped second order system, PD is a phase detector, k_e is the feedback gain and $\omega_e(t)$ is the frequency estimate. The external input to the system $x(t)$ is assumed to be in the form

$$x(t) = A_1 \cos\left[\omega_0 t + \theta_1(t)\right], \tag{5.1}$$

where $A_1 > 0$ is the amplitude and ω_0 is the nominal angular frequency, both of which are assumed to be constant but unknown quantities. The instantaneous phase of $x(t)$

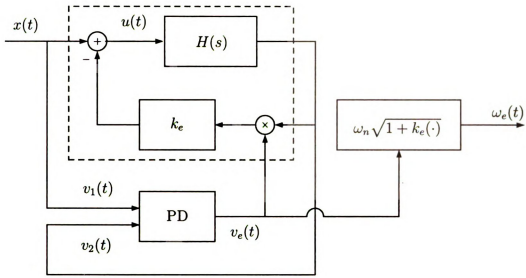

Figure 5.2. Model of the frequency estimator system.

is $\theta_1(t)$. Thus, the instantaneous frequency of the input is

$$\omega_s(t) = \omega_0 + \dot{\theta}_1(t). \tag{5.2}$$

The transfer function of the lightly damped second order system can be expressed as

$$H(s) = \frac{\omega_n^2}{s^2 + 2\zeta\omega_n s + \omega_n^2}, \tag{5.3}$$

where ω_n is the natural frequency of this system and ζ is the damping ratio. The dashed box represents the closed loop system, the resonant frequency of which is adjusted to match the instantaneous frequency of the input. The signal $v_e(t)$ is the error generated by the phase detector, which is assumed to be an exor type. Following analysis similar to that developed earlier in this thesis, $v_e(t)$ is given by

$$v_e(t) = f_e(t) * \varphi\left[\theta_2(t) - \theta_1(t)\right], \tag{5.4}$$

where $f(t)$ is the impulse response of the lowpass filter and $*$ is the convolution operation.

With $v_e(t)$ known, it then follows from Figure 5.2 that

$$u(t) = x(t) - k_e v_e(t) v_2(t). \tag{5.5}$$

Thus, the closed loop system within the dashed box is governed by the differential equation

$$\ddot{v}_2(t) + 2\zeta\omega_n \dot{v}_2(t) + [1 + k_e v_e(t)]\,\omega_n^2 v_2(t) = \omega_n^2 x(t), \tag{5.6}$$

where the resonant frequency of this closed loop system is

$$\omega_e(t) = \omega_n \sqrt{1 + k_e v_e(t)}. \tag{5.7}$$

Hence, the closed loop resonant frequency $\omega_e(t)$ can be easily computed from the output of the phase detector $v_e(t)$, and provided to the PLL as an estimate of the input frequency.

5.3 Analysis and Design

Consider the frequency estimator system shown in Figure 5.2. Here it can be easily seen how the frequency estimate $\omega_e(t)$ can be computed when provided the error signal $v_e(t)$. However, as good performance of this system requires careful design of the lowpass filter and lightly damped second order system, equations that describe the dynamics of this system are necessary. Following analysis methods similar to those provided earlier in this thesis, the nonlinear equation that describe the dynamics of

the frequency estimator system with an exor type phase detector is

$$\frac{\omega_e^2(t) - \omega_n^2}{\omega_n^2} = f_e(t) * k_e k_\theta \arctan\left[\frac{\omega_s^2(t) - \omega_e^2(t)}{2\zeta\omega_n\omega_s(t)}\right]. \tag{5.8}$$

Simulations show that (5.8) represents the actual frequency extimator system very accurately. However, a simpler model is still desired for design purposes. After linearization, the the simplified linear time-invariant model of the resonance tuning system becomes

$$\delta\omega_e(t) = f_e(t) * k\left[\delta\omega_s(t) - \delta\omega_e(t)\right], \tag{5.9}$$

where $k = k_e k_\theta/(2\zeta)$. The block diagram of the system described by this equation is as shown in Figure 5.3. This linear model describes the actual system accurately,

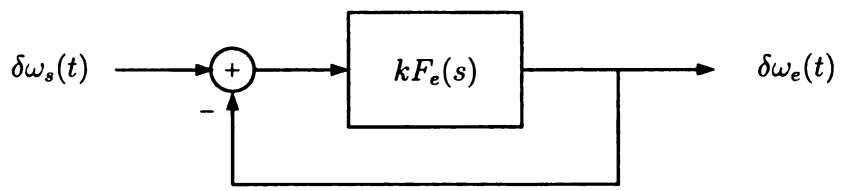

Figure 5.3. Simplified model of the resonance tuning system.

provide that

$$\frac{|\delta\omega_s(t) - \delta\omega_e(t)|}{\zeta\omega_n} \leq \frac{1}{2}. \tag{5.10}$$

However, as the goal of the enhanced PLL is to achieve lock to an input with unknown frequency, whether this condition is satisfied or not, will most likely remain unknown as well. Despite this fact, (5.9) is still a valuable tool in that it provides a starting point for design process.

5.4 Simulation

In this section, the enhanced PLL system is simulated to demonstrate its lock range capabilities. All simulations were performed in MATLAB/Simulink.

In order to determine whether the output signal $y(t)$ has locked to the input signal $x(t)$, the frequency-phase error between these two signals must be calculated. This error is defined as

$$\phi(t) = [\omega_s(t) - \omega_e(t)]\, t - k_p \int_0^t v_p(\tau) d\tau, \tag{5.11}$$

where $\omega_s(t)$ is the instantaneous input frequency, $\omega_e(t)$ is the instantaneous estimator frequency, k_p is the PLL gain and $v_p(t)$ is the PLL phase detector error. Thus, when $y(t)$ locks to $x(t)$, $\phi(t)$ approaches zero. Lock also occurs when $\phi(t) = n\pi$, where $n = 1, 2, 3, ...$

Using the methods described above, three simulations are performed. In the all three simulations, the lightly damped second order system is assumed to have natural frequency $\omega_n = 1000$ rad/s and damping ratio $\zeta = 1$. The gain of the frequency estimator is chosen as $k_e = 25$, while the gain of the PLL is $k_p = 50$. The phase detector of both the frequency estimator and PLL is an exor type, with logic level V chosen as ± 5V. The filter of the PLL is defined as

$$F_p(s) = -\frac{1}{(s+10)}, \tag{5.12}$$

while the filter of the frequency estimator is

$$F_e(s) = \frac{1}{s(s+25)}. \tag{5.13}$$

For comparison purposes, a standard PLL is also included in the first two simulations, with the same parameters as PLL portion of the enhanced PLL.

In the first simulation, the input signal $x(t)$ is given a nominal frequency of $\omega_0 = 1010$ rad/s and phase of $\theta_1(t) = 0$. The results are shown in Figure 5.4 and Figure 5.5, where Figure 5.4 is a plot of the frequency - phase error $\phi(t)$ versus time and Figure 5.5 is a plot of the actual input and output signals $x(t)$ and $y(t)$. In both figures, the enhanced PLL system and the standard PLL are represented by the solid and dashed lines, respectively. In Figure 5.5, the dotted line represents the input signal $x(t)$. From these figures, it is clear that enhanced PLL locks both in frequency and phase, while the standard PLL locks in frequency, but with some steady state phase error.

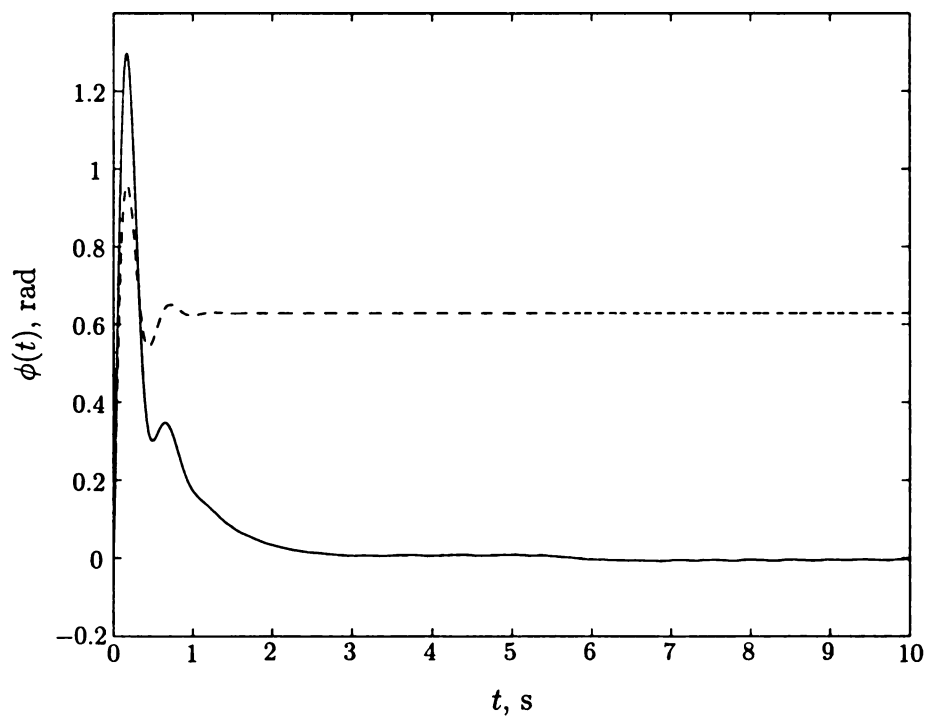

Figure 5.4. Frequency-phase error results with small initial frequency difference.

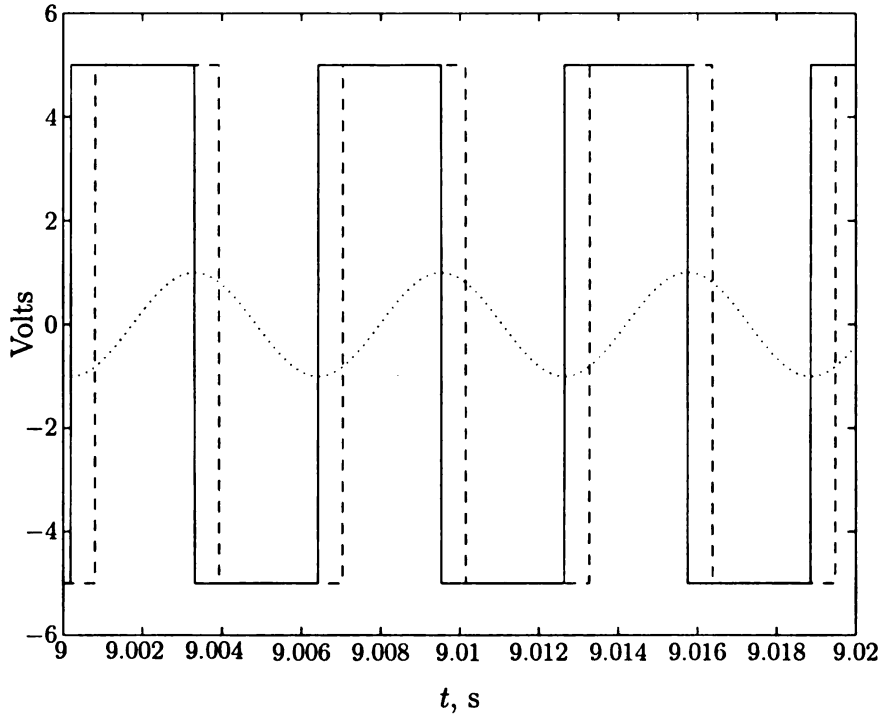

Figure 5.5. Input and output signals with small initial frequency difference.

As is the case with most problems in engineering, increased performance of one aspect of a problem usually requires a decrease in the performance of another aspect of the problem. This tradeoff holds true for the enhanced PLL, as seen from the steady state oscillations in Figure 5.4. However, it will be shown in the next two simulations that the lock range of the enhanced PLL dramatically exceeds that of the standard PLL.

In the second simulation, the input nominal frequency is increased to $\omega_0 = 1100$ rad/s. The phase is still chosen as $\theta_1(t) = 0$. The results are shown in Figure 5.6 and Figure 5.7. Again, the solid line and dashed lines represent the enhanced PLL system and standard PLL, respectively, while in Figure 5.7, $x(t)$ is represented by the dotted line. From these figures it is clearly visible that the range of the standard PLL is exceeded, while the enhanced PLL still achieves lock.

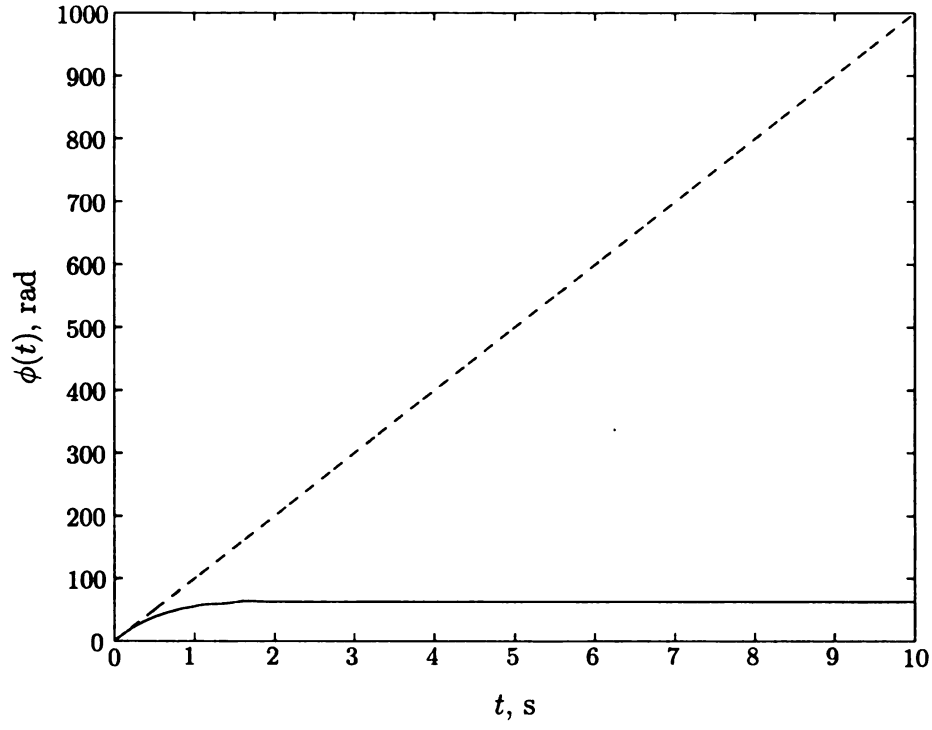

Figure 5.6. Frequency - phase error results with $\omega_0 = 1100$ rad/s.

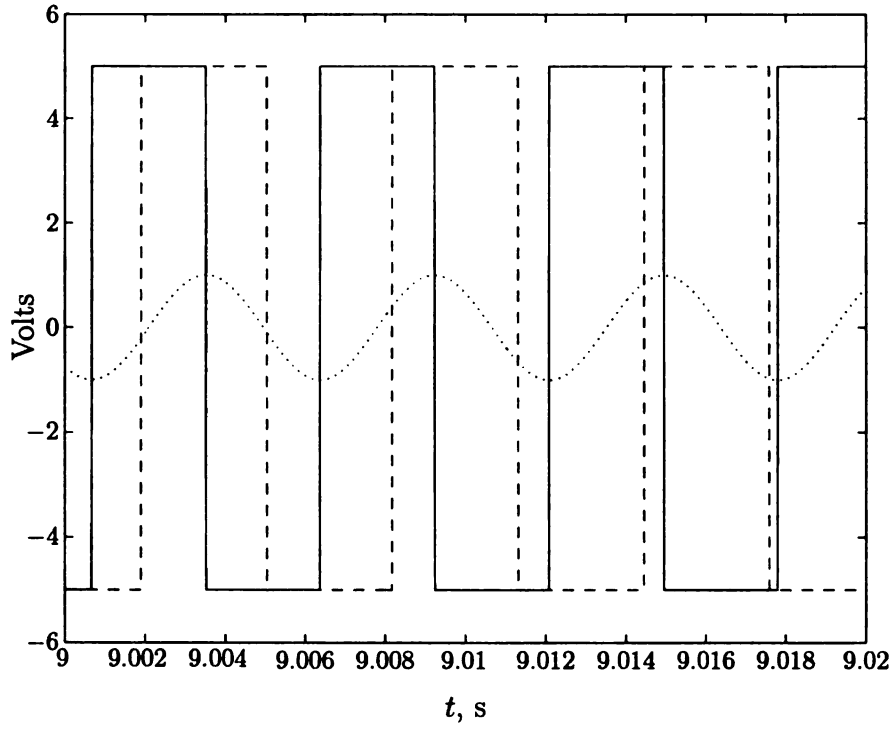

Figure 5.7. Input and output signals with $\omega_0 = 1100$ rad/s.

To demonstrate the capabilities of the enhanced PLL, a third simulation is performed with the input frequency chosen as $\omega_0 = 4000$ rad/s, and the phase $\theta_1(t) = 0$. The results are shown in Figure 5.8 and Figure 5.9. These figures show that the extend PLL can achieve lock despite an input frequency four times as large as its nominal frequency.

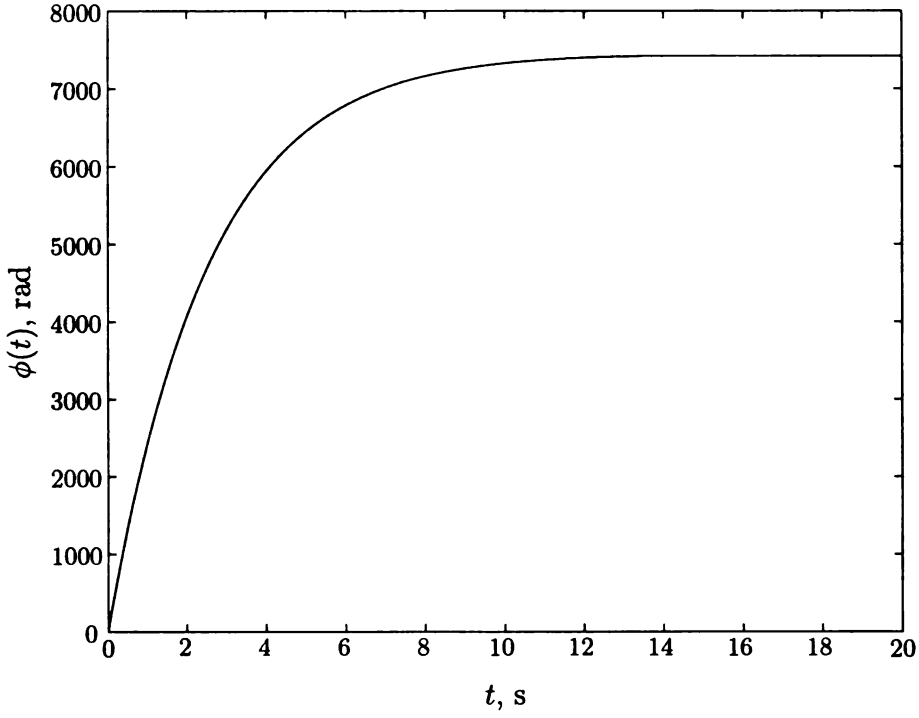

Figure 5.8. Frequency - phase error result with $\omega_0 = 4000$ rad/s.

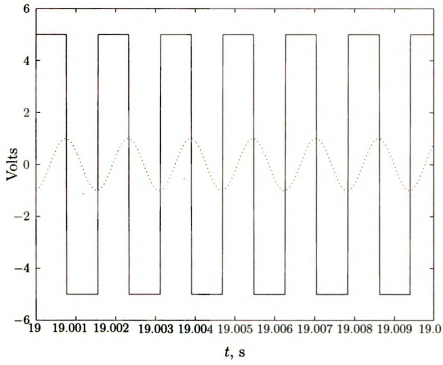

Figure 5.9. Input and output signals with $\omega_0 = 4000$ rad/s.

Based on the simulations presented here, initial results of an adaptive method to enhance the capabilities of the phase locked loop are promising.

CHAPTER 6

Conclusions

6.1 Summary

Resonant systems arise in many areas of science and engineering. Some examples include ultrasonic motors, piezoelectric transducers, induction heating loads, some resonant inverter loads, microelectromechanical gyroscopes, cavity resonators and cyclotrons. For optimal performance, these systems must be excited at their resonant frequencies. However, even if resonant and excitation frequencies are initially matched, over time these frequencies can shift due to disturbances such as temperature or humidity change, load variation, manufacturing variability, fatigue damage, microphonics and electromagnetic detuning, resulting in a loss of performance. This mandates employment of a resonance tuning control system that maintains lock between the excitation frequency and the resonant frequency.

Three resonance tuning systems for lightly damped second order passive loads have been investigated in this thesis. Each method uses the error between the excitation and resonant frequencies to adaptively match these frequencies. This error is obtained with a phase detector. In the first method, a voltage controlled oscillator provides the excitation to the load. The excitation frequency is adaptively tuned by providing the error signal from the phase detector to the voltage-controlled oscillator. The second method adaptively tunes the resonant frequency of the resonator by changing its structure, such as geometry or element values. Finally, the third method uses proportional feedback around the resonator and adaptively adjusts the feedback gain

to tune the closed loop resonant frequency to the excitation frequency.

Assuming that the parameters of the lightly damped second order system are slowly time-varying, nonlinear time-varying models that accurately predict the performance of each resonance tuning system have been developed. These developed models were subsequently linearized to obtain linear time-invariant models that facilitate both analysis and design of the resonance tuning systems. Based on the developed linear time-invariant models, guidelines for designing the resonance tuning systems were also provided. The results were illustrated through simulations.

6.2 Future Work

Despite the research of resonance tuning systems with phase detectors presented in this thesis, there still exist many unanswered questions and thus the need for future research work on these systems. For instance, analysis of the effects of noise on these systems is still required. Also, more work is needed toward developing solid nonlinear design guidelines, for applications where the linear models do not provide an accurate representation of the actual system. Also, research is required for the development of these adaptive resonance tuning systems for higher order resonators.

BIBLIOGRAPHY

BIBLIOGRAPHY

[1] Y. Mizutani, T. Suzuki, H. Ikeda, H. Yoshida, and S. Shinohara, "Frequency control of MOSFET fullbridge power inverter for maximizing output power to megasonic transducer at 3 MHz," *Proc. IEEE Ind. Applicat. Conf.*, St. Louis, MO, pp. 1644–1651, 1998.

[2] S. Furuya, T. Maruhashi, Y. Izuno, and M. Nakaoka, "Load-adaptive frequency tracking control implementation of two-phase resonant inverter for ultrasonic motor," *IEEE Trans. Power Electron.*, **7**, pp. 542–550, 1992.

[3] A. Arnau, T. Sogorb, and Y. Jiménez, "A new method for continuous monitoring of series resonance frequency and simple determination of motional impedance parameters for loaded quartz-crystal resonators," *IEEE Trans. Ultrason., Ferroelect., Freq. Contr.*, **48**, pp. 617–623, 2001.

[4] J. Phinney and D. J. Perreault, "Filters with active tuning for power applications," *IEEE Trans. Power Electron.*, **18**, pp. 636–647, 2003.

[5] Y. S. Kwon, S. B. Yoo, and D. S Hyun, "Half-bridge series resonant inverter for induction heating applications with load-adaptive PFM control strategy," *Proc. IEEE Appl. Power Electron. Conf. and Expo.*, Dallas, TX, pp. 575–581, 1999.

[6] R. P. Leland, "Adaptive mode tuning for vibrational gyroscopes," *IEEE Trans. Contr. Syst. Technol.*, **11**, pp. 242–247, 2003.

[7] X. Sun, R. Horowitz, and K. Komvopoulos, "Stability and resolution analysis of a phase-locked loop natural frequency tracking system for MEMS fatigue testing," *ASME J. Dynamic Syst, Meas. Contr.*, **124**, pp. 599–605, 2002.

[8] S. I. Kwon, A. Regan, and M. Prokop, "Frequency shift observer for an SNS superconducting RF cavity," *IEEE Trans. Nucl. Sci.*, **50**, pp. 201–210, 2003.

[9] S. Simrock, G. Petrosyan, A. Facco, V. Zviagintsev, S. Andreoli, and R. Paparella, "First demonstration of microphonic control of a superconducting cavity

with a fast piezoelectric tuner," *Proc. IEEE Particle Accel. Conf.*, Hamburg, Germany, pp. 470–472, 2003.

[10] P. Cevc, T. Walczak, and H. M. Swartz, "Whole body L-band resonator with a wide range frequency tuning using piezo actuator," *Current Topics in Biophysics*, **26**, pp. 15–19, 2002.

[11] M. Liepe, W. D. Moeller, and S. N. Simrock, "Dynamic Lorentz force compensation with a fast piezoelectric tuner," *Proc. IEEE Particle Accel. Conf.*, Chicago, IL, pp. 1074–1076, 2001.

[12] C. Hovater, J. Delayen, L. Merminga, T. Powers, and C. Reece, "RF control requirements for the CEBAF energy upgrade cavities," *Proc. Int. Linac Conf.*, Monterey, CA, pp. 518–520, 2000.

[13] J. R. Delayen, "Electronic damping of microphonics in superconducting cavities," *Proc. IEEE Particle Accel. Conf.*, Chicago, IL, pp. 1146–1148, 2001.

[14] F. Braun and W. Arnold, "Fast matching of load changes in the ion cyclotron resonance frequency range," *Proc. IEEE Sympo. Fusion Engin.*, Albuquerque, NM, pp. 395–398, 1999.

[15] K. Akai, N. Akasaka, E. Ezura, T. Kageyama, H. Mizuno, F. Naito, H. Nakanishi, Y. Takeuchi, Y. Yamazaki, and T. Kobayashi, "Tuning control and transient response of the ARES for KEKB," *Proc. IEEE Particle Accel. Conf.*, Sitgas, Spain, pp. 1994–1996, 1996.

[16] T. Sümesağlam, A. İ. Karşılayan, "A digital approach for automatic tuning of continuous-time high-Q filters," *IEEE Trans. Circuits Syst. II*, **50**, pp. 755–761, 2003.

[17] C. Gökçek, "Disturbance rejection and reference tracking in control systems with saturating actuators," Ph.D. dissertation, University of Michigan, 2000.

[18] C. Gökçek, "Tracking the resonance frequency of a series RLC circuit using a phase locked loop," *Proc. IEEE Conf. Contr. Appl.*, Istanbul, Turkey, pp. 609–613, 2003.

[19] J. A. Jeltema, J. Ma, C. Gökçek, "Analysis and design of resonance tuning systems," *Proc SPIE Optics East*, Philadelphia, PA, 2004.

[20] J. A. Jeltema, Gökçek, "Adaptive Resonance Tuning through Feedback," *Proc. American Cont. Conf.*, Portland, OR, 2005.

[21] J. A. Jeltema, Gökçek, "Adaptively Enhanced Phase Locked Loops," *Proc. IEEE Conf. Contr. Appl.*, Toronto, Ontario, 2005.

[22] C. A. Desoer and E. S. Kuh, *Basic Circuit Theory*, McGraw-Hill, NY, 1969.

[23] B. C. Kuo, *Automatic Control Systems*, Prentice Hall, NJ, 1987.

[24] J. L. Stensby, *Phase Locked Loops*, CRC Press, NY, 1997.

[25] F. M. Gardner, *Phaselock Techniques*, Wiley, NY, 1979.

[26] E. W. Kamen, P. P. Khargonekar, and A. Tannenbaum, "Control of slowly-varying linear systems," *IEEE Trans. Automat. Contr.*, **34**, pp. 1283–1285, 1989.

[27] C. A. Desoer, "Slowly varying system $\dot{x} = A(t)x$," *IEEE Trans. Automat. Contr.*, **14**, pp. 780–881, 1969.

[28] M. Freedman and G. Zames, "Logarithmic variation criteria for the stability of systems with time varying gains," *SIAM J. Contr.*, **6**, pp. 487–507, 1968.

[29] B. A. Francis and W. M. Wonham, "The internal model principle for linear multivariable regulators," *Appl. Math. Optim.*, **2**, pp. 170–194, 1975.

[30] H. K. Khalil, *Nonlinear Systems Analysis*. NJ: Prentice-Hall, 2002.